BRNO UNIVERSITY OF TECHNOLOGY
VYSOKÉ UČENÍ TECHNICKÉ V BRNĚ

FACULTY OF MECHANICAL ENGINEERING
FAKULTA STROJNÍHO INŽENÝRSTVÍ

INSTITUTE OF MATHEMATICS
ÚSTAV MATEMATIKY

HEAT TRANSFER SOLUTION OF SOLIDIFYING STEEL SYSTEM WITH PHASE CHANGE WITH MOVING EDGE CONDITIONS

ŘEŠENÍ PŘENOSU TEPLA TUHNOUCÍ OCELOVÉ SOUSTAVY SE ZMĚNOU FÁZE PŘI POHYBUJÍCÍCH SE OKRAJOVÝCH PODMÍNKÁCH

MASTER'S THESIS
DIPLOMOVÁ PRÁCE

AUTHOR — **Bc. Tomáš Fedorko**
AUTOR PRÁCE

SUPERVISOR — **prof. Ing. Josef Štětina, Ph.D.**
VEDOUCÍ PRÁCE

BRNO 2019

BRNO UNIVERSITY OF TECHNOLOGY
FACULTY OF MECHANICAL ENGINEERING

Specification Master's Thesis

Department:	Institute of Mathematics
Student:	**Bc. Tomáš Fedorko**
Study programme:	Applied Sciences in Engineering
Study field:	Mathematical Engineering
Leader:	**prof. Ing. Josef Štětina, Ph.D.**
Academic year:	2018/19

Pursuant to Act no. 111/1998 concerning universities and the BUT study and examination rules, you have been assigned the following topic by the institute director Master's Thesis:

Heat transfer solution of solidifying steel system with phase change with moving edge conditions

Concise characteristic of the task:

Theoretical analysis of the possibility of the numerical solution of a 3D solidifying steel system of a rectangular cross–section with a 2D moving slice. It is a comparison of different approaches to solving the significant nonlinearity of the solved equation due to the inclusion of latent heat. The functional numerical model should be able to simulate the real continuous casting of steel.of the calculation.

Goals Master's Thesis:

The current state of the art in the use of 2D numerical models with variable boundary conditions simulating the movement of the system. Developing a model in a MATLAB environment with the including of a real geometry of caster and cooling of the blank. Processing of various approaches to solving the inclusion of high non–linearity of the thermo–physical properties of the steels during solidification and cooling eg using enthalpy method, specific heat method, and temperature recovery method. Mutual comparison of these methods in terms of numerical precision, suitability for different methods of time discretization for non–stationary problems and parallelization.

Recommended bibliography:

BIRAT, J. P., et al. The Making, Shaping and Treating of Steel: Casting Volume: 11th. Edition. Alan W. Cramb. Pittsburgh, PA, USA: The AISE Steel Foundation, 2003. 1000 s. ISBN 0-930767-04-7.

INCROPERA, F., DEWITT, D., BERGMAN, T., LAVINE, A. Principles of heat and mass transfer. 7th ed., international student version. Singapore: John Wiley, c2013, xxiii, 1048 s. ISBN 978-0-470-64-15-1.

IRVING, W. R. Continuous casting of steel. The Institute of Materials, 1993. ISBN 0 901716537.

STEFANESCU, D. M. Science and Engineering of Casting Solidification, Second Edition, Springer Science, 2009. 412 s. ISBN 978-0-387-74609-8.

Deadline for submission Master's Thesis is given by the Schedule of the Academic year 2018/19

In Brno,

L. S.

prof. RNDr. Josef Šlapal, CSc. Director of the Institute	doc. Ing. Jaroslav Katolický, Ph.D. FME dean

Abstract

The master's thesis aim is to develop a 2D numerical slice model with moving boundary conditions of real geometry of caster in MATLAB environment. The model deals with a high non-linearity of the thermo-physical properties of steel during solidification and cooling. Not only the non-linearity of thermo-physical properties, but also the non-linearity during phase change is handled and simulated. Phase change is modeled by enthalpy method, effective heat capacity method and temperature recovery method. In the end, comparison of different approaches from the perspective of accuracy, speed of the computation and suitability of time discretization for non-stationary problems and parallelization is derived.

Abstrakt

Cílem diplomové práce je vytvoření 2D numerického modelu pohybujícího se řezu s proměnnými okrajovými podmínkami skutečné geometrie plynulého odlévání a chlazení předlitku v prostředí MATLAB. Model se zabývá vysoce nelineárními termofyzikálními podmínkami oceli během tuhnutí a chlazení. V práci je simulovaná nejen nelinearita termofyzikálních podmínek, ale také nelinearita při fázové změně. Fázová změna je modelovaná pomocí metody entalpie, metody zdánlivé kapacity a metody teplotního zotavení. Všechny výsledky práce jsou porovnány z více hledisek, jako např. z hlediska přesnosti, rychlosti výpočtu, nebo vhodnosti časového diskretizačního kroku pro nelineární problémy, a paralelizace.

Keywords

Continuous casting, heat transfer, mold, latent heat, 2D slice model, enthalpy method, effective heat capacity method, temperature recovery method, finite difference method, explicit method, error.

Klíčová slova

Plynylé odlévání, prenos tepla, krystalizátor, latentní teplo, 2D model pohybujícího se řezu, metoda entalpie, metoda zdánlivé kapacity, metoda teplotního zotavení, metoda konečných diferencí, explicitní metoda, chyba.

FEDORKO, T. *Heat transfer solution of solidifying steel system with phase change with moving edge conditions*: Master's thesis. Brno: Brno University of Technology, Faculty of Mechanical Engineering, Institute of Mathematics, 2019. 64 p. Supervised by prof. Ing. Josef Štětina, Ph.D.

I declare that I have written my Master's thesis *Heat transfer solution of solidifying steel system with phase change with moving edge conditions* on my own, under the guidance of my supervisor prof. Ing. Josef Štětina, Ph.D., and using the sources listed in references.

May 24, 2019 Tomáš Fedorko

I would like to express my sincere gratitude to my supervisor prof. Ing. Josef ŠTĚTINA, Ph.D. for supervising my Master's thesis, for all his support, patience, advice, suggestions and valuable comments.

I would also like to thank Ing. Tomáš Mauder, Ph.D. for his help with coding, advice and suggestions. Next, I would like to thanks Ing. Michal Březina for motivating me to not surrender.

My special thanks belong to my parents, siblings and my love Lucie for their support, understanding, patience and prayers.

Tomáš Fedorko

Contents

1 Introduction

Steel is the kind of material that we simply could not imagine our lives without. It is so ubiquitous, an average person takes it for granted and does even not think about the entire complicated process that the steel has to go through in order to be turned from raw ore to final product. One of the many necessary steps on this long path is the process of casting, which melts the material in order to mold it into a shape that can be used further down the pipeline of different manufacturing procedures, which then turn it into the finished product.

Although simple to define, the actual process of casting is quite difficult and sensitive to many different interfering factors. It is a delicate act of striking the right balance between quality, production speed, production costs and other factors.

For many decades the only option for industry innovators to improve on the casting process were physical experiments and observation, which are time consuming and costly. Luckily, huge hardware and software advancements of the recent years coupled with knowledge in the field of numerical modeling open up a whole array of new alternatives

The goal of this thesis is to analyse several numerical methods, namely the enthalpy method, the effective heat capacity method and the temperature recovery method and evaluate their fit for solving the problem of continuous casting of steel from the point of accuracy, suitability for different methods of time discretization in non-stationary problems and parallelization.

The first chapter of this thesis presents a very short excursion into the history of continuous casting along with a modest description of the process itself. Subsequent chapter expands more on the details of the casting process and describes the key parts involved. Next is the description of the mathematical model of casting. Theoretical background of the modeling methods is layed down in this chapter together with the description of the various types of boundary conditions that need to be taken into account by these methods. The fifth chapter discusses the translation of the mathematical model defined previously into its counterpart numerical model that can then be calculated on a computer. And finally the last two chapters present the implementation of the numerical methods described and the discussion of the results achieved in this work.

2 Continuous Casting

This chapter presents to readers a short introduction of continuous casting, its history, brief description and basic principles. Most of the historical facts, pictures and graphs used here were found in [2], [5].

2.1 Historical background

For more than a century, the traditional method of conversion of steel from the liquid phase to the solid phase was by use of ingot molds, where each ingot was cast independently [5]. The number of ingots from a single ladle of liquid steel depended on the ladle size and the size of each ingot individually. After the steel within the ingot mold had solidified the ingots were removed and charged into the soaking pits, so they could be reheated for rolling to semi-finished or finished products. As early as the nineteenth century the attraction of using a more continuous method was recognized and some of the methods were applied to casting of non-ferrous metals with low melting points. But not in the case of steel due to many technical problems related to higher temperatures involved and low thermal conductivity of steel [5]. The first significant attempt at continuous casting was direct strip casting by Sir Henry Bessemer in 1856, where he poured liquid metal in his double roller apparatus, which he used to cast thin strips for brass powder manufacture as shown in Figure 1. However, he did not pursue this technology, presumably giving higher priority to developing the steelmaking process first [2].

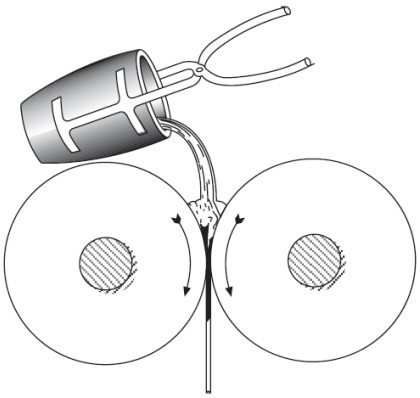

Figure 1: Attempt at direct strip casting by Henry Bessemer in 1856 [2].

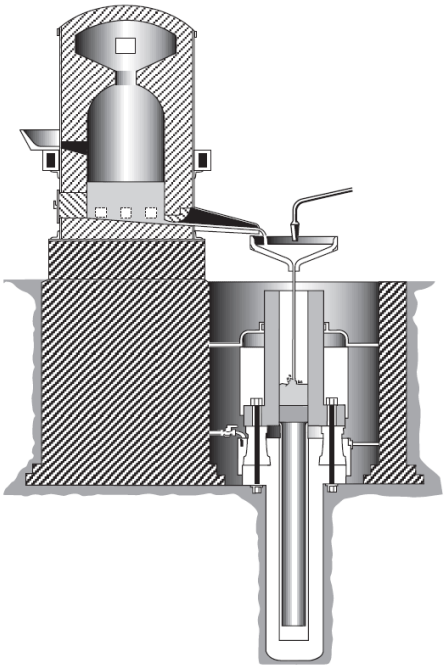

Figure 2: Stoppered tundish and ingot mold with hydraulic ram applied by H. Bessemer [2].

Later he implemented a tundish with stopper for slag retention as shown in Figure 2. The 10×10 inch mold below the tundish got a hydraulic ram to push the ingot upward for a direct rolling of the ingot without reheating. The very first apparatus resembling a

conventional continuous casting machine was presented by Benjamin Atha in 1901. The water-cooled mold was directly connected with the tundish, while the strand induced a claw-shaped head and was withdrawn intermittently by a pair of driven rolls (see Fig. 3) [2]. Further in the text, a continuous casting machine will be abbreviated as CCM.

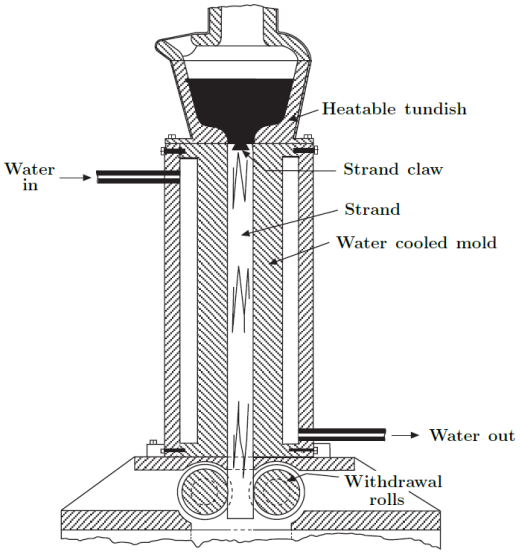

Figure 3: First billet casting apparatus by B. Atha [2].

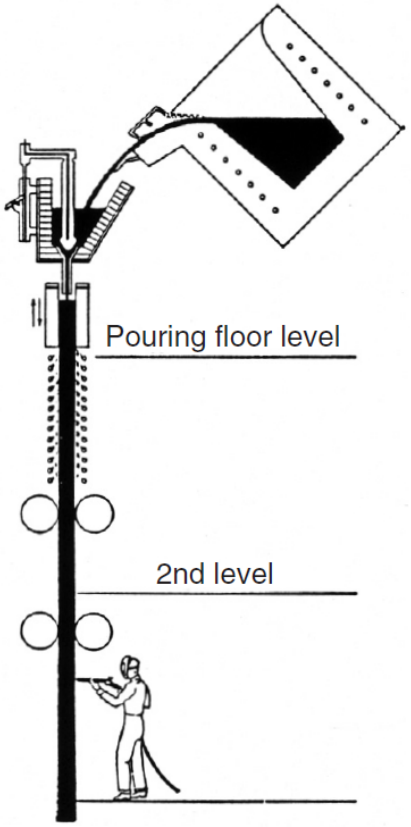

Figure 4: Scheme of the first caster for steel with a production guarantee with lip pouring from an induction furnace into a stoppered tundish [2].

It was discovered that with steel some considerable problems occurred. Due to sticking of steel to the mold wall, relative motion between the metal being cast and mold wall was required. It was not until 1933 when Siegfried Junghans developed and patented his mold oscillation system that set the foundations for the large scale application of the process of continuous casting of steel [5]. Due to Second World War, the semi-industrial pilot plants began to emerge for the continuous casting of steel. One of the first constructed machines was a vertical caster installed in 1946 for the production of steel billets at Low Moor in Great Britain (see Fig. 4) [5]. Later on, in 1951 twelve casters of this type were operating in the world, mostly in Germany and USA (5 machines) and in the Great Britain (2 machines). In 1968, company VOEST-ALPINE created a new type of machine focused on a high quality of the final product. Between 1970 – 1990, more improvements on the CCMs were made, which brought the higher quality and productivity. For instance, a faster exchange between ladle and tundish, adjustable mold width, cooling by water-air nozzles, electro-magnetic blending, temperature monitoring, whole covering of liquid steel between ladle and tundish feeding, tundish and mold feeding and many others. Increasing

the production of steel by continuous casting method brought arise of interest in research and innovation. Worldwide production of steel by continuous casting is displayed in graph (see Fig. 5). We can see that the worldwide production of steel by this method is increasing because of the costs, quality, speed and overall variability in production of specific and desirable steel.

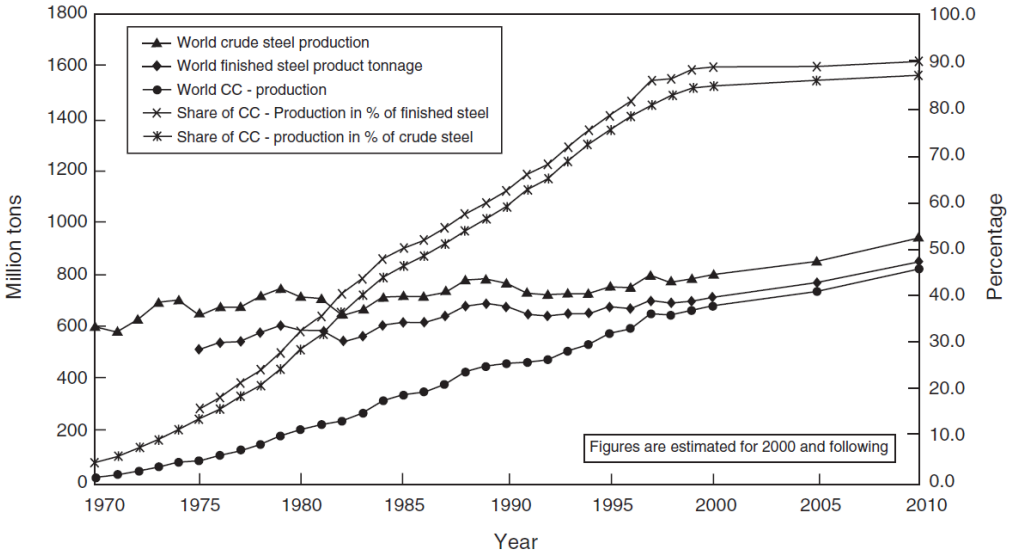

Figure 5: Evolution of world steel production and share of continuous casting [2].

2.2 Brief description of continuous casting process

The basic principle of the continuous casting process for steel is based on teeming liquid steel vertically into a water cooled copper mold which is open at the bottom [5]. Heat transfer to the water-cooled copper solidifies the liquid steel and a solid skin is formed, which increases in thickness down the length of the copper mold. Two very fundamental principles are required to avoid sticking of the solidifying skin to the copper mold [5].

1. The mold moves downward faster than the solidifying skin for a percentage of the oscillating cycle.
2. A lubricant has to be provided as an interface between solidifying skin and copper mold. Before 1970, rapeseed oil had been used for almost every caster and it is still used for smaller billet size, where a refractory submerged nozzle cannot be used. On most of other machines a synthetic casting powder is used on a top of the metal in the mold [5]. The powder in contact with the liquid steel melts and fills the gap between the solidifying skin and the mold.

As soon as the skin on the liquid steel is sufficiently thick to contain the liquid steel, the strand leaves the mold and is further cooled by water or water-air nozzles. The reason why it is further cooled by nozzles and not by copper mold is that cooling by mold is less efficient in heat transfer due to the air gap forming between the mold wall and the solidified skin. Therefore, it is more efficient to use direct water spraying from high pressure nozzles [5]. However, if the solidified skin is unconstrained or unsupported, it cannot withstand the pressure arising from the liquid steel and would bulge outwards. Therefore, it is necessary to support the solidifying skin by rollers or other mechanical system (see Fig. 6) [5].

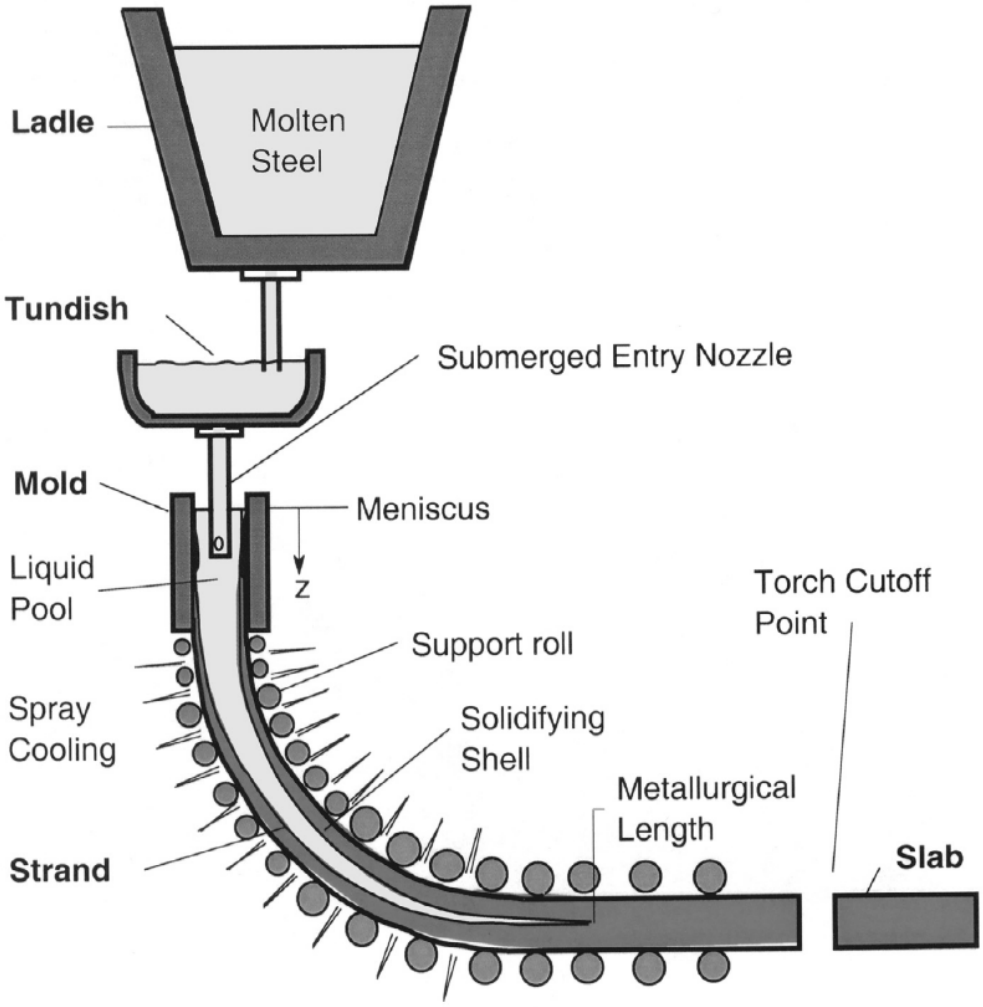

Figure 6: Scheme of continous casting [2].

The principle of modern CCM can be briefly described in a following way. A liquid steel is initially teemed from the steelmaking vessel into the ladle. The ladle is lifted onto the CCM and supported by either ladle car or ladle turret. The liquid steel is than poured from the ladle into the tundish by way of sliding valve mechanism and the stream is protected by a refractory tube to avoid any reoxidation from the atmosphere [5]. For modern CCMs, it is common that they operate in parallel, so the steel can be poured into the tundish, whose main purpose is to distribute steel over a number of casting strands and to provide more help in the control of pouring the liquid steel into the continuous casting mold.

The tundish design and its configuration depends on a number of strands and distance between the strands [5]. The strand becomes completely solid after passing several meters down the machine. The exact position when strand is completely solid depends on casting speed, cooling conditions and the product thickness. The strand is straightened by use of rollers and at the position, where it becomes horizontal, it is withdrawn by the power of driven rolls. To enable a fully solidified strand to be withdrawn at horizontal position, the slab is cast on a curvature, the radius of which depends on several factors connected with product dimension and quality requirements [5]. At the end, a fully solidified strand is cut by torch machine which travels at the same speed as strand and cuts it transversely to its original position.

It has to be said that solidified shell leaving the mold is relatively weak and any excessive friction in the mold or any decreasing in the shell thickness due to uneven cooling can lead to breakout. The breakouts are very expensive and undesirable, because they lead to interruption of the casting. In fact, this is time consuming, since the machine needs to be recovered from the results of spilled molten steel. It is often required to change the mold and top zone during the breakouts. Much work has been carried out to avoid breakouts and to have rapid recovery time when they do occur.

3 Parts of the casting process

This chapter details the process of continuous casting, namely the main parts of caster and its different cooling zones. The several expressions, i.e., a heat transfer, heat flow and heat transfer coefficient, are derived herein the chapter. These expressions will be required later in the text, namely for a mathematical model of continuous casting. The following text was inspired by [2], [5], [11], [14].

3.1 Steel supply and tundish operation

To ensure a suitable return of initial investment, the CCM is required to operate at high production rates while achieving high surface and internal quality standards for steel semi-products. To achieve high production rates, it is necessary to cast a large number of ladles in sequence without stopping the casting process. The sequence ratio can vary with respect to the circumstances, which are influenced by product size and quality mix.

If the product grade and size mix allow a sequence ratio of at least 10 ladles, the tundish may become a limiting factor in achieving the sequence level [5]. The tundish is limited mostly by erosion, or blockage of submerged entry nozzle, or stopper rod to the mold. To achieve a high productivity and high quality of the steel, it is essential that ladles of steel are supplied to the CCMs with the exact temperature at precise time. Usually in a practice, a ladle drain time is equal to the time of steel making furnace.

From a ladle to a tundish liquid steel, teeming is controlled by the use of sliding gate valve consisting of three refractory plates, where one of them can be moved by hydraulic ram. By continuously weighting and measuring the tundish, steel level in tundish and its whole operation can be controlled automatically. Automatic control along with other automatic process control systems can lead to reduced manning requirements [5]. Control in tundish and protection from oxidation of the teeming stream was neglected and their importance underestimated. However, during the 1970s, it was discovered that the key to maintain clean and quality products depends on them. Hence, they are important to maintain specific limits for quality reasons and to enhance mold metal level control.

Due to the low pressure generated in the sliding gate nozzle and the refractory tube, there is a great risk of sucking in air between them. To solve this problem, various systems (considering the inert gas is utilized as a sort of gas shroud protection) are used. In addition to reoxidation protection, the prevention of a slag flow from ladle to tundish on emptying the ladle is of great importance too (especially for sequence casting). During the casting process, the systems for a slag detection are used, and as soon as the slag appears, they should close the ladle gate (to ensure the slags will not build up in the tundish) [5].

As was mentioned before, one of the main purposes of tundish is to distribute the liquid steel over the appropriate number of continuous casting strands. Another ones are, e.g., supporting the removal of inclusions from the steel and acting as a reservoir during the ladle changing, while enabling the casting under the required conditions. To accomplish the above purposes, an adequate volume and depth of the tundish must be ensured. Additionally, an internal arrangement of weirs and dams is used to facilitate inclusion removal and increase the residence time of steel in tundish [5].

There is used a cover powder on the top of liquid steel in tundish to insulate and reduce the radiative heat loss and to absorb the inclusions, which float out of steel

[5]. For a further reduction of heat losses, a refractory lined lids are used on both ladles and tundishes [5].

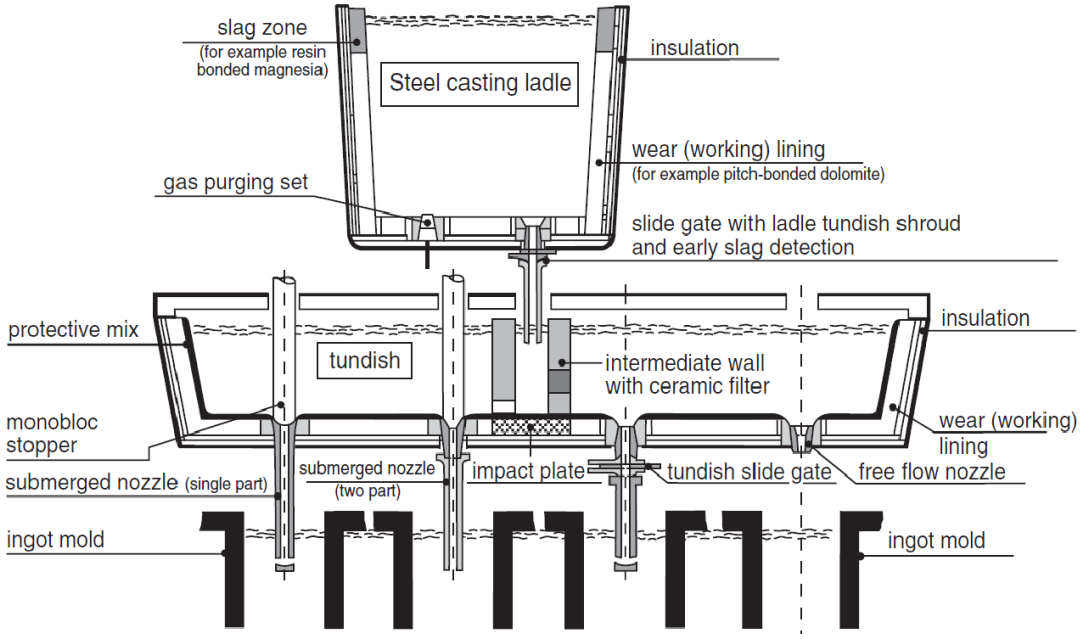

Figure 7: Scheme of the ladle and tundish [2].

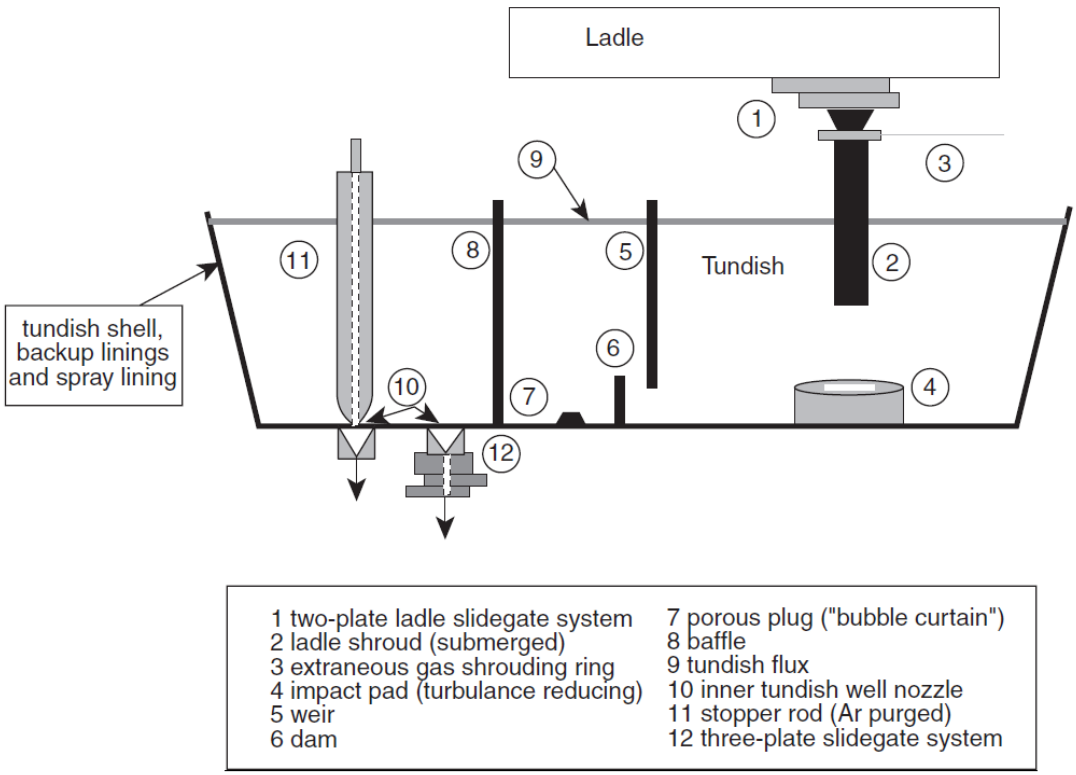

Figure 8: Scheme of the tundish [2].

Flow of the liquid steel from tundish to the mold and meniscus level in the mold are controlled either by sliding gate mechanism (similar to the one between ladle and tundish) or by a stopper rod. With slide gate mechanism we may have to flood the whole system with inert gas in order to prevent any air penetration (to prevent any undesirable reoxidation of the steel). Also, it is necessary to maintain the variation of level of the liquid steel in the mold at minimum, since high variation of meniscus level in the mold has a significant effect on strand surface quality.

3.2 Mold

A mold (or the first cooling zone) is the only mechanical part of three cooling zones of caster, which is in direct contact with molten steel. It is probably the most important part of the machine and it has to operate under several conditions. Particularly, it needs to create a homogeneous shell by efficient uniform heat transfer [5]. The mold is a part that has to be long lasting, capable of quick change of section size and it has to require minimum maintenance effort.

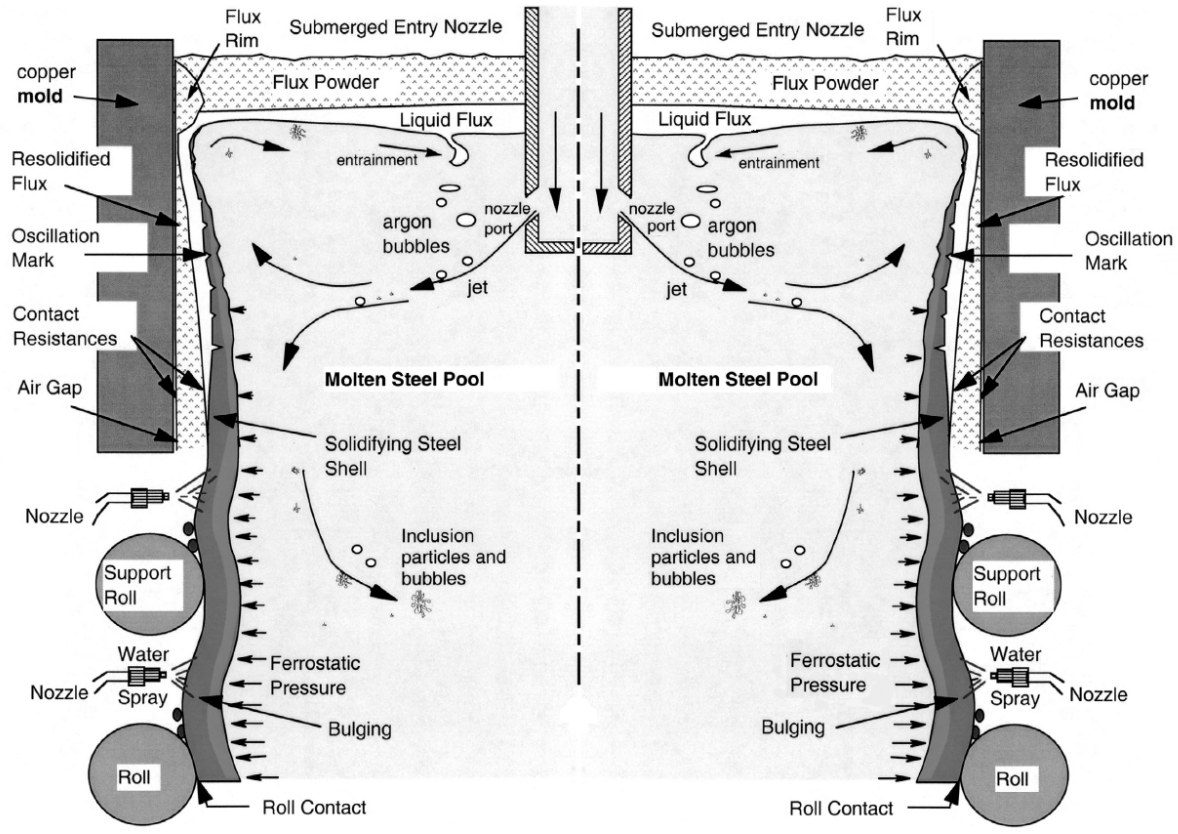

Figure 9: Mold scheme and phenomenas of first cooling zone [2].

Molds are cooled by a high quality water, usually demineralized and supplied for a recirculating system [5]. The fail systems and design are usually arranged to provide minimum water flow velocity in the cooling chase of 8m/s. Normal mold length was (until recently) 700 mm, but the range expands from 500 to 1200 mm [5]. The most recent trend has been towards 900 mm mold, which provide increased solidified skin at

the mold outlet, where the casting speeds are higher. Appropriate rate between length and casting speed is depicted in figure below (see Fig. 10).

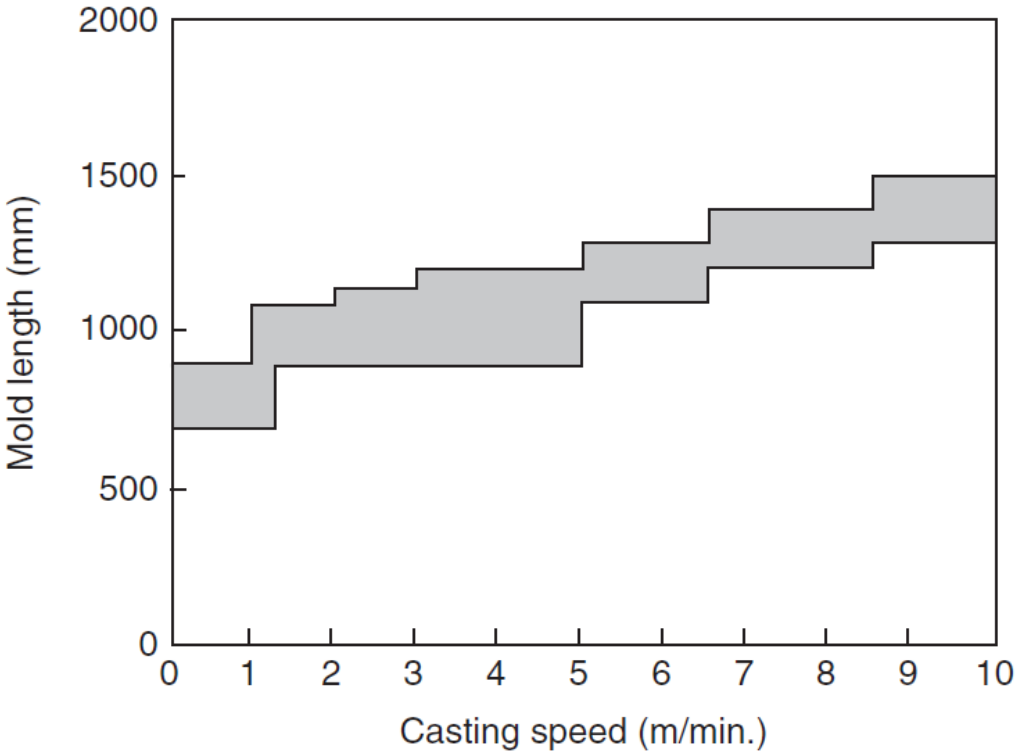

Figure 10: Appropriate length over a speed ratio (depicted as grey area) [2].

In the past, it was believed that the heat transfer is enhanced by close mold to shell contact of a fixed nonmoving mold. Even with the Junghans type mold oscillation, no relative movement was imparted during a downward motion, extending over three quarters of total cycle [2]. As this impeded lubricant infiltration, negative strip mold oscillation was introduced. Negative strip oscillation means moving the mold slightly faster than the strand during the downstroke of the cycle. This has been vital to minimize shell sticking under the conditions of imperfect mold level control prevailing at that time, since any shell defect may easily lead to shell tearing under the effect of mold friction [2]. Much more safety is anticipated from a meniscus free mold technology, which would permit strand withdrawal without lubrication and without oscillation, however practically feasible solutions are still to be developed [2].

A control of mold friction by rapeseed oil was found to be quite effective, provided that oil losses due to burning were retarded by an oil flash point exceeding the mold wall temperature. This has favored the development of tabular molds with relatively thin wall. Nevertheless, when mold powders were invented in the 1960, they immediately became more popular. They proved to be more effective and stable technology to keep mold friction low and strand surface quality high. However, in the transition to mold powders usage, it had been overlooked that convectional mold level sensors were not compatible and only steel level detection by electromagnetic sensing were viable [2]. Also mold powder performance is assured only by continuous powder feeding in order to maintain a stable layer of liquid slag on the top of steel level. Today, the fully automatic powder feeders are

still exemption clause, even though the process has been simplified by gravity feeding of granular powders (see Fig. 11). Thus, the surface defects, as well as breakouts, are still to a large extent manmade by manual mold powder feeding at irregular intervals.

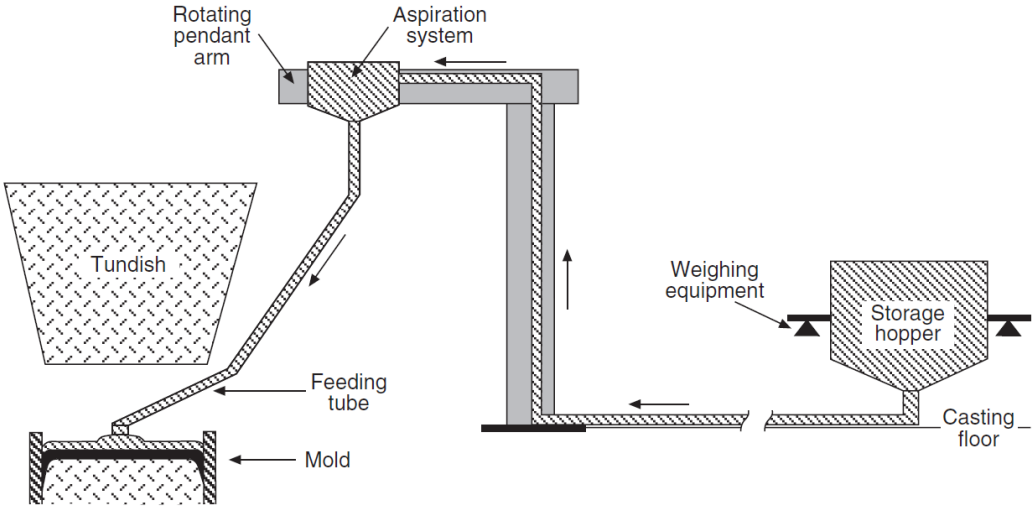

Figure 11: Scheme of gravity-type feeder for granular powder with powder consumption control [2].

Heat transfer in a mold is the combination of convection, conduction and radiation, and proportionally to the rest of cooling zones (more about them later), we get that the biggest heat transfer occurs in the mold. Namely, around 10% - 30% of total heat is drained from the strand. In fact, the heat transfer from a strand surface is a multivariable function depending mostly on casting speed, chemical composition and mold design [11]. We can consider it as a serial connection of thermal resistors, where the biggest branch lies in the gap (see Fig. 12).

Let us denote a density of heat flow as $\dot{q}$ and let us introduce it by

$$\dot{q} = \frac{T_{\text{surf}} - T_w}{R}, \tag{1}$$

where T_{surf} is the temperature on a surface of the strand, T_w is the temperature of cooling water and R is a total heat resistance. We can express the total heat resistance as

$$R = \frac{1}{htc_w} + \frac{\mathrm{L}_{Cu}}{k_{Cu}} + \frac{\mathrm{L}_{steel}}{k_{steel}} + \frac{\mathrm{L}_p}{k_p}, \tag{2}$$

where L_i is an appropriate thickness of mold areas, depicted in Figure 12, and k_x is an appropriate thermal conductivity. Namely, by i we consider either *steel* (mold covering), Cu (mold copper wall) or p (mold powder). A coefficient htc_w is a heat transfer coefficient for cooling water. We can derive htc_w from Nusselt number for a pipe flow

$$\mathrm{Nu} = \frac{htc_w D}{k} = 0,026\,\mathrm{Re}^{0,8}\,\mathrm{Pr}^{1/3}\left(\frac{\eta}{\eta_l}\right)^{0,14}, \tag{3}$$

where D is a hydraulic diameter, k is thermal conductivity, $\left(\frac{\eta}{\eta_l}\right)$ is a viscosity term and Re, Pr are Reynolds number and Prandtl number, respectively. For more about these parameters and numbers, see [3].

For more accurate result we have to include also a radiant part of density of heat flow in the gas gap. Let $\dot{q}_r$ be a flow of radiant part, given by

$$\dot{q}_r = \frac{\sigma \left(T_{\text{surf}}^4 - T_m^4\right)}{\varepsilon_{\text{surf}}^{-1} + \varepsilon_m^{-1} - 1}, \tag{4}$$

where σ is Stefan–Boltzmann constant, ε_m and $\varepsilon_{\text{surf}}$ are emissivities of mold and strand's surface, respectively. Then, by adding (1) to (4), we get a total dencity of heat flow $\dot{q}_{total}$ given by

$$\dot{q}_{total} = \dot{q} + \dot{q}_r = \frac{T_{\text{surf}} - T_w}{R} + \frac{\sigma \left(T_{\text{surf}}^4 - T_m^4\right)}{\varepsilon_{\text{surf}}^{-1} + \varepsilon_m^{-1} - 1}. \tag{5}$$

Hence, the heat flow $\dot{Q}$ through one side of the mold may be obtained by integration of total density of heat flow through this side. In other words, we get

$$\dot{Q} = \int_0^{\mathrm{L}x} \int_0^{\mathrm{L}z} \dot{q}_{total} \, dzdx, \tag{6}$$

where L_x and L_z denotes width and length of the mold, respectively.

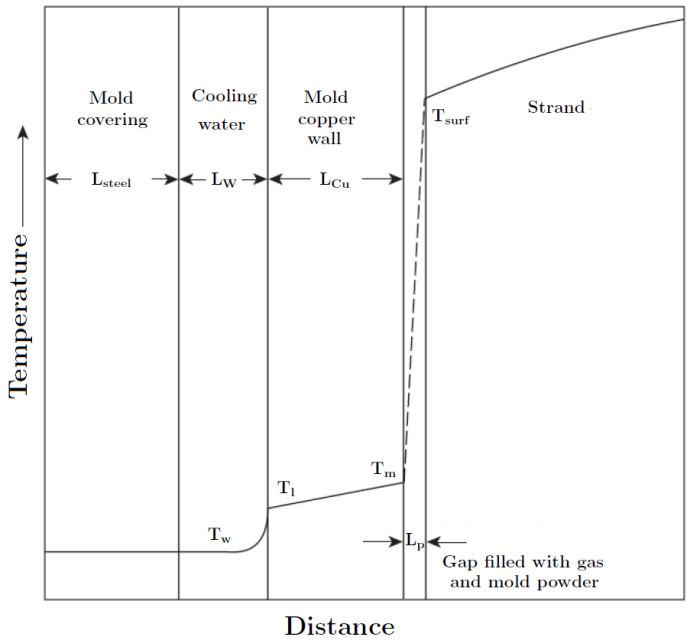

Figure 12: Temperature evolution between surface of the strand and cooling water of the mold [2].

Another way of calculating the heat flow from the mold is to measure inflow and outflow water temperature. Heat flow from the strand is than expressed by

$$\dot{Q} = \dot{Q}_w + \dot{Q}_{Cu} + \dot{Q}_{lp}, \tag{7}$$

where $\dot{Q}_w$ is the heat flow for cooling water, $\dot{Q}_{Cu}$ is the heat flow for mold copper wall and $\dot{Q}_{lp}$ is the heat flow by mold powders. Usually, the percentage distribution of heat flows are 5% by copper mold walls, 8% by mold powders. Moreover, the heat flow by cooling water is explicitly given by:

$$\dot{Q}_w = \dot{V}_w \left[\rho_w \left(T_{\text{out}}\right) c_w \left(T_{\text{out}}\right) T_{\text{out}} - \rho_w \left(T_{\text{in}}\right) c_w \left(T_{\text{in}}\right) T_{\text{in}}\right], \tag{8}$$

where ρ_w is a water density, c_w is a specific heat capacity of water, T_{out} and T_{in} are temperatures in outflow and inflow, respectively. However, the total heat flow in the mold is not distributed equally. In fact, it is a function of position and casting speed.

3.3 Secondary cooling zone

After the strand leaves the mold, it enters the secondary cooling zone. The strand with partially solidified shell requires both mechanical support and continual cooling. Mechanical support is required because of the ferrostatic pressure of the liquid steel and without it the strand would quickly bulge outwards. For the cooling control of the strand, high pressure water-air nozzles (or water nozzles) are used, but also water cooled mechanical support extract heat from the strand as well. Radiation also contributes to the total heat transfer [5]. The design and operation of secondary cooling system highly depends on the shape of the strand that being cast, section size and overall configuration of the whole CCM.

The number of support rolls vary for billet, bloom or slab casters and it also depends on casting speed. Billets are small square sections, usually up to 150 mm square or with a diameter up to 150 mm. Blooms are square or rectangular sections greater than 150 mm up to 800 mm x 400 mm with aspect ratio usually less than 2. Slabs are anything larger than blooms with aspect ratio bigger than 2. For illustration, see Figure 13.

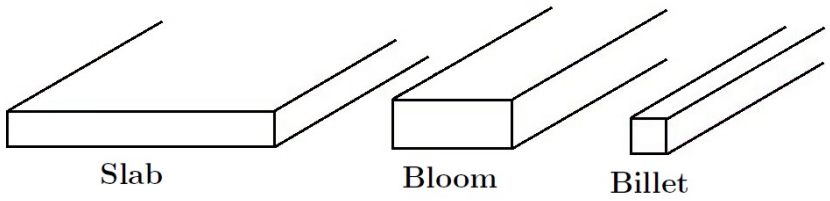

Figure 13: Scheme of the strand types.

For higher casting speeds, more support rolls may be required. For the larger billet and bloom casters (or casters with higher casting speed), there is an increased propensity of bulging, since the shell is still not so strong, and the support rolls have to be extended further down the strand.

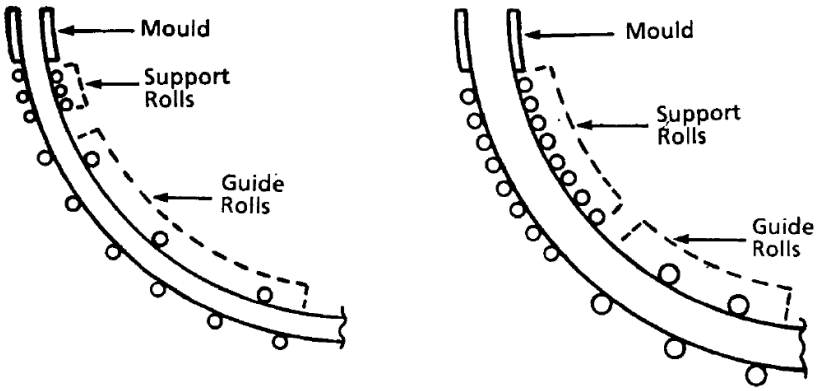

Figure 14: Support rolls for billet or bloom casting [5].

For slab machines, the bulging of the broad faces extends to the point, where solidification is complete and invariably strand support of the wide faces extends the full length of the machines [5]. For slab casters, support systems are arranged into the segments, where each segment consists of three to six pairs of rolls and has the ability to rapidly exchange the whole segment. The segment frames are clamped together by hydraulic cylinders and the roll gaps are preset using chocks and shims [5]. Water nozzles are attached and aligned on the headers, so they can spray water in between rolls and therefore, cool the strand.

All the segments are fixed to the frame of the caster, where the inner radius of rolls can be adjusted by the hydraulic cylinders to enable a change of casting thickness (or for full opening). Full opening is required in the case of an overcooled slab in the machine, which has to be removed by cutting or for scheduled maintenance of the segments in the original place [5].

In fact, obtaining the total heat transfer in secondary cooling zone is a quite difficult task. The main processes, which contribute to total cooling are:

1. Cooling due to radiation.
2. Cooling due to water nozzles by evaporating of the water droplets and water accumulated under the roller.
3. Cooling due to the rolls conduction.

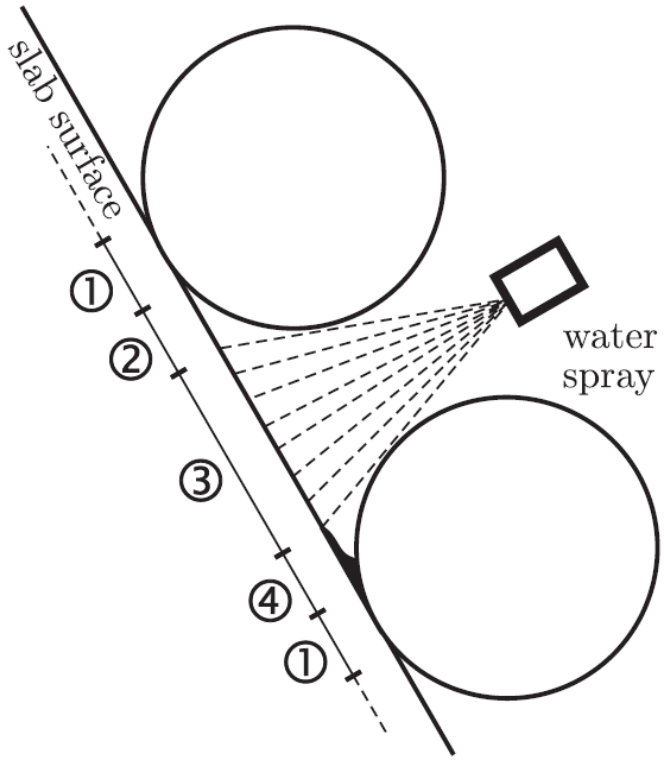

Figure 15: Scheme of the heat transfer in the secondary cooling zone: (1) Rolls conduction (2) natural convection and radiation (3) forced convection under the nozzle (4) water interflow and water accumulation [14].

Before the 1980, only water nozzles were used for continuous casting of steel. However, in the early 1980, the water-air nozzles were introduced. They consist of both the water and air supply to a nozzle at high pressure resulting in much finer water particles whilst

also having a wide angle [5]. The smaller particle size has the advantage of increasing the heat transfer coefficient and more uniform application of water.

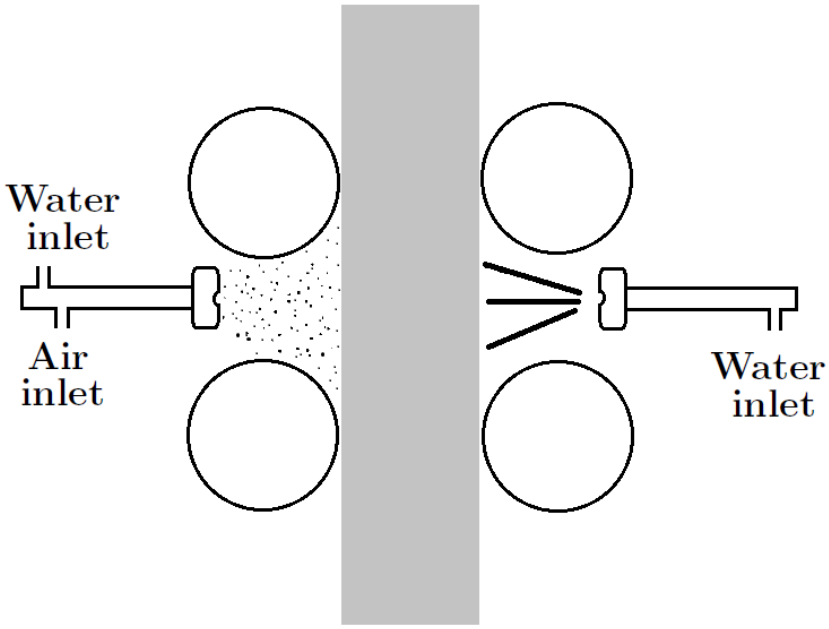

Figure 16: Sketch of the water and water-air nozzle.

To set a density of heat flow under the nozzle can be quite a difficult process. Here, an important role plays a Leidenfrost effect. We can express it by

$$\dot{q} = htc\left(T_{\text{surf}} - T_w\right) + \varepsilon_{\text{surf}}\sigma\left(T_{\text{surf}}^4 - T_w^4\right), \tag{9}$$

where htc denotes heat transfer coefficient under the nozzles, $\varepsilon_{\text{surf}}$ emissivity, the Stefan–Boltzmann constant is set as $\sigma = 5.67051 \cdot 10^{-8}$, T_{surf} and T_w is again the temperature on the strand surface and temperature of cooling water, respectively. The density of heat flow outside of the nozzles is the sum of natural convection and radiation:

$$\dot{q} = htc_{nat}\left(T_{\text{surf}} - T_\infty\right) + \varepsilon_{\text{surf}}\sigma\left(T_{\text{surf}}^4 - T_\infty^4\right), \tag{10}$$

where T_∞ denotes ambient temperature and htc_{nat} is natural heat transfer coefficient.

In the point, where strand touches the supporting rolls, we observe the heat flow density, which is described by

$$\dot{q} = \frac{\pi\frac{l}{2}d\left(htc_{rol}\left(T_{rol} - T_\infty\right) + \varepsilon_{rol}\sigma\left(T_{rol}^4 - T_\infty^4\right)\right)}{S} + \dot{q}_{ak}, \tag{11}$$

where S is the area of strand/roll contact, $\dot{q}_{ak}$ is the density of heat flow from water interflow and water accumulation. Note that for all of the above equations, we can express the emissivity by empiric relation

$$\varepsilon = 0,78828571429 + 0,0003375\left(T_{\text{surf}}\right) - 40,17857143 \cdot 10^{-8}\left(T_{\text{surf}}^2\right),$$

or

$$\varepsilon = \frac{0,85}{\left[1 + \exp\left(42,68 - 0,02682T_{\text{surf}}\right)^{0,0115}\right]}.$$

For determining the heat transfer coefficient for the rollers, we can omit its rotation due to its small angular speed and use the formula for turbulent runaround of horizontal roll [11]. Hence, we get

$$htc_{rol} = \frac{\mathrm{Nu}\, k_{air}}{D}, \tag{12}$$

where $\mathrm{Nu} = 0,1\,(\mathrm{Pr}_{air}\,\mathrm{Gr})^{1/3}$ is Nusselt number, Pr_{air} is Prandtl number and $\mathrm{Gr} = \dfrac{g\beta_{\mathrm{air}}\,(T_{\mathrm{surf}} - T_\infty)\,D^3}{\nu_{\mathrm{air}}^2}$ is Grashof number (for more about this numbers, see [3]).

The heat transfer coefficient htc_{nat} (for natural convection) can be expressed by

$$htc_{nat} = 0,84\,(T_{\mathrm{surf}} - T_\infty)^{1/3}. \tag{13}$$

As we suggested before, the hardest part is a determination of the heat transfer coefficient under the nozzles. Its value depends on a density of water flow, temperature of the strand etc. In particular,

$$htc = 708W^{0,75}T_{\mathrm{surf}}^{-1,2} + 0,116, \tag{14}$$

where W denotes density of water flow and T_{surf} is a surface temperature. More relations can be found in [2], [3], [4].

In general, the heat transfer coefficients stated above are sufficient only for a number of nozzles, temperatures and water flows. Therefore, if we want to obtain a suitable results of our mathematical model, the knowledge of experimental data is required.

3.4 Third cooling zone

The last part of CCM is the so-called third cooling zone. The strand is carried by transport rolls to the cutting machine. The cutting machine can be mechanical or oxygen powered torch machine. The machine moves with the same speed as strand and cuts it transversely.

In the third cooling zone, there is no further cooling by nozzles, and heat transfer occurs only in the form of natural convection and radiation given by (10), considering the natural heat transfer coefficient (13). Nevertheless, the computation is not so simple and the heat transfer is pretty complex in reality. For instance, during a parallel casting, a heat from the other strands has to be considered.

4 Mathematical model of continuous casting

Herein the chapter, a mathematical model of continuous casting is derived. The following text is supported by [2], [3], [6], [11], [12].

In recent years, decreasing computational costs and the increasing power of commercial modelling packages and numerical methods allow application of mathematical models as an additional tool to physical models to understand and to model complex phenomena in continuous casting. Nevertheless, because of the enormous complexity of this process, it is impossible to simulate all the phenomena at once. We need to make a reasonable assumptions and neglect less important processes, which does not affect the model in a significant way. Because the mechanical and structural properties of the steel depend on a temperature field, we will assume that heat and mass transfer play the main role in our model. We will take a closer look at modelling of the temperature field, which from the point of view of thermodynamics is a 3D heat, mass transfer with phase and structural changes.

A general 3D heat transfer equation that describes the temperature distribution inside of the solidifying body is based on the solution of the Fourier-Kirchhoff equation

$$\frac{\partial}{\partial t}[\rho(T)c(T)T] = \nabla[k(T)\nabla T] + \mathbf{v}\nabla[\rho(T)c(T)T] + Q^*, \tag{15}$$

where $\nabla = \left(\frac{\partial}{\partial x}, \frac{\partial}{\partial y}, \frac{\partial}{\partial z}\right)$ is the nabla operator, $\mathbf{v} = [v_x, v_y, v_z]$ is the velocity vector and Q^* is the term combining all internal heat sources during phase or structural changes. Therefore, a temperature depending on time and position $T(x, y, z, t)$ is obtained as a result of the equation (15). Since the main heat transfer is due to conduction, we can assume that the velocity vector has only part expressing the velocity of the strand down the machine v_z. Hence, we have

$$\frac{\partial}{\partial t}[\rho(T)c(T)T] = \nabla[k(T)\nabla T] + \frac{\partial}{\partial z}\left[v_z\rho(T)c(T)T\right] + Q^*. \tag{16}$$

In general, the thermal conductivity $k(T)$ varies in each direction. In our case, let us assume that we have a homogeneous material. Therefore, we can rewrite the equation (16) as

$$\frac{\partial}{\partial t}[\rho(T)c(T)T] = k(T)\Delta T + \frac{\partial}{\partial z}\left[v_z\rho(T)c(T)T\right] + Q^*, \tag{17}$$

where $\Delta = \left(\frac{\partial^2}{\partial x^2} + \frac{\partial^2}{\partial y^2} + \frac{\partial^2}{\partial z^2}\right)$ is the Laplace operator. Equation (17) is in Cartesian coordinates, where for radial part it is more convenient to transform it to cylindrical coordinates r and φ. After transformation, the equation (17) has the form

$$\frac{\partial}{\partial t}[\rho(T)c(T)T] = k(T)\Delta T + \frac{\partial}{\partial \varphi}\left[\frac{1}{r}v_z\rho(T)c(T)T\right] + Q^*, \tag{18}$$

where $\Delta T = \frac{1}{r}\frac{\partial}{\partial r}\left(r\frac{\partial T}{\partial r}\right) + \frac{1}{r^2}\frac{\partial^2 T}{\partial \varphi^2} + \frac{\partial^2 T}{\partial x^2}$. In all of the above equations, one may obtain Q^* expressed by

$$Q^* = \rho(T)L\frac{\partial f_s}{\partial t}, \tag{19}$$

where L is latent heat and f_s denotes the ratio between solid and liquid phase in the mushy zone. Let us assume that in the mushy zone, f_s depends only on the temperature.

Therefore, we get

$$Q^* = \rho(T) L \frac{\partial f_s}{\partial T} \frac{\partial T}{\partial t}. \tag{20}$$

If there is no explicit relation between the solid fraction and the temperature (or the solid fraction cannot be easily evaluated as a function of temperature), the linear model is generally used, which yields (see [12]) to

$$\begin{aligned} f_S &= 1 && T \leq T_S \\ f_S &= \frac{T_L - T}{T_L - T_S} && T_S \leq T \leq T_L \\ f_S &= 0 && T \geq T_L \end{aligned} \tag{21}$$

From the all of above equations (15) – (20), we can see that results are directly connected to thermophysical properties of certain material. These properties depend on the temperature, which complicates calculations and whole problem.

The first of the thermophysical properties is a thermal conductivity $k(T)$. It expresses how a certain material is able to conduct heat. It reaches the high values for metals and usually lowers down with increasing temperature. In computations, it is always advantage to have the experimental data of steel compound. However, if the data are not available, there is a possibility to get them from a regression relation

$$k(T) = 58.676491 + T\left[-0.051443 + T\left(2.320847 \cdot 10^{-5} + T\left(-9.405061 \cdot 10^{-11}\right)\right)\right]. \tag{22}$$

The next thermophysical property is a density $\rho(T)$, which actually describe a fraction of mass and size of a certain object. The density is given by $\rho = \frac{m}{V}$, or $\rho = \frac{\sum M_i x_i}{V_m}$ for compound materials, where M_i is a molar mass, V_m is a molar volume and x_i is a volume fraction of the i-th component. Again, if the experimental data are not available, we are possible to get them from a regression relation of steel

$$\rho(T) = 7.870498 \cdot 10^3 + T\left[-0.448171 + T\left(2.642733 \cdot 10^{-4} + T\left(-1.550589 \cdot 10^{-7}\right)\right)\right]. \tag{23}$$

The last, but the most important property is a specific heat capacity $c(T)$, which describes the amount of heat required for heating up of one kilogram of material by one kelvin. We can express it by $c = \frac{Q}{m\Delta T}$, or by $c = \frac{m_1 c_1 + m_2 c_2 + \ldots + m_n c_n}{\sum m_i}$, if we have consider a material compound of more substances with masses $m_1, m_2, \ldots, m_n$ and special heat capacities $c_1, c_2, \ldots, c_n$. Note that every substance with decreasing temperature reduces specific heat capacity. Therefore, we have to include temperature dependency to our model. Either we can use experimental data, or we can compute them from regression relation of steel

$$c(T) = 392.035678 + T\left[1.12188 + T\left(-1.163574 \cdot 10^{-3} + T\left(3.785874 \cdot 10^{-7}\right)\right)\right]. \tag{24}$$

4.1 IDS program

The equations (22), (23), (24) stated above in preceding section are specifying some of the basic regression relations of thermophysical properties of the steels. However, these relations are providing just approximate results. In fact, their match with real properties

depends on a chemical compound of the specific steel. Therefore, the usage of preceding relations is very unfortunate for general computations of temperature field. However, there is another way how to get the right data for a specific steel compound. It is based on the usage of experimental detection of every property we need. Nevertheless, such an approach is very expensive and time consuming due to vast selection of steel compounds.

Nowadays, the most common tool used for obtaining the thermal properties of steels is the IDS program, which numerically computes segregating, structural and chemical processes. IDS was developed in 1984 in Helsinki. It operates on a combination of empiric and physical approaches. It computes properties such as density, enthalpy, thermal conductivity, specific heat capacity, viscosity, solid and liquid temperature etc. Results of this program were experimentally tested for many steels with different chemical compounds and satisfactory results were obtained. We will use this program to get the data required for the numerical computations. More about this program can be found in [13].

4.2 Initial and boundary conditions

Notice that solution of the equations (15) – (20) is highly dependent on initial and boundary conditions. To obtain a unique solution to such a problem, we need to specify more than just the governing differential equation [3]. We have to specify these boundary conditions and by forcing the solution to satisfy them we would obtain the unique solution. Since the model's differential equation has no room for other information, we need to supply them as separate conditions. In general, an initial condition can be characterized in following way:

$$T(x, y, z, t = 0) = T_{\text{initial}}(x, y, z) = T_{\text{casting}}. \tag{25}$$

Usually, T_{casting} is setted as a constant for the whole domain, for continuous casting its value is equal to the value of casting temperature or, more precisely, the temperature of liquid metal, which goes from tundish to mold.

To describe a heat transfer problem completely, two boundary conditions must be given for each direction of the coordinate system along which the heat transfer is significant [3]. Thus, we need two initial conditions for 1D problem, four of them for 2D problem etc. Next, the most typical boundary conditions are going to be described.

4.2.1 Specified temperature boundary condition

As a first type of boundary conditions, let us introduce a so-called Dirichlet boundary condition. It prescribes a temperature condition on boundary (see Fig. 17). A temperature on the exposed side can be easily and directly measured. Therefore, one of the easiest ways to define a thermal condition on the surface is to specify the temperature [3]. For instance, to specify heat transfer through 1D wall of length L, the conditions will look like:

$$\begin{aligned} T(0, t) &= T_1 \\ T(\mathrm{L}, t) &= T_2 \end{aligned} \tag{26}$$

where T_1 and T_2 are our prescribed temperatures. These can also vary in time.

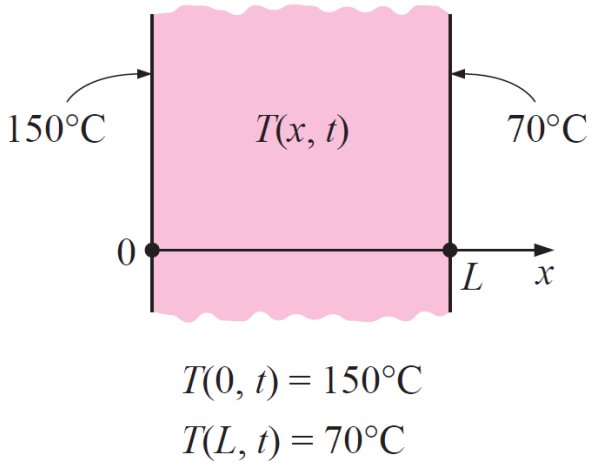

Figure 17: Dirichlet boundary conditions on both sides [3].

4.2.2 Specified heat flux boundary condition

The next introduced boundary condition is so-called Neumann's condition. It prescribes a condition when we have the information about energy interactions at a surface (Fig. 18) . This information may be used to determine the heat flux and therefore, the boundary condition using Fourier's law of heat conduction:

$$\dot{q} = -k\frac{\partial T}{\partial x}. \tag{27}$$

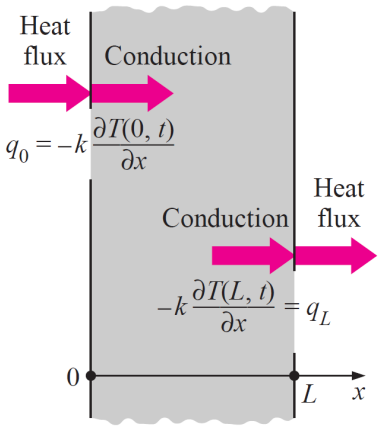

Figure 18: Neumann boundary condition on both surfaces of a plane wall [3].

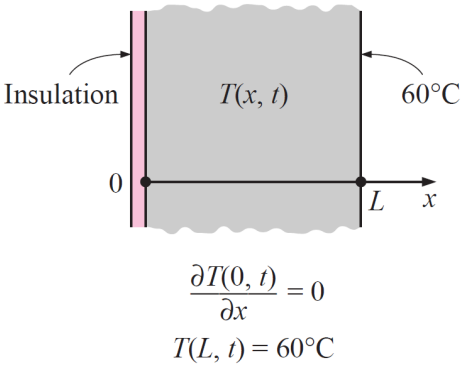

Figure 19: Wall with insulated and Dirichlet boundary condition [3].

Such an boundary condition is obtained, when the specific heat flux is setted to $-k(\partial T/\partial x)$. We have to keep in mind that the sign of specific heat flux is very important. If the sign is positive, then the heat flux and coordinate axis have the same direction. On contrary, if it is a negative value, the converse of preceding sentence is considered to be true. Moreover, if there occurs a mix of these signs, the boundary will interpret heat gain as heat loss and vice versa.

We will suggest some special cases of boundary condition. Firstly, the one with insulated boundary (see Fig. 19). In fact, the insulation does not eliminate a heat transfer totally, unless it is infinitely thick, but proper insulated wall. If it is so, it will reduce the heat transfer through itself to negligible values. Therefore, such an condition can be modeled as:

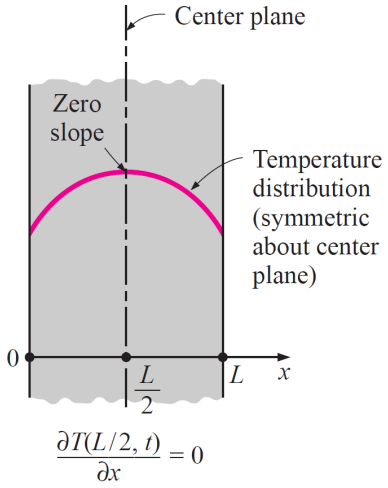

$$-k\frac{\partial T(0,t)}{\partial x}=0. \tag{28}$$

Figure 20: Thermal symmetry at $x = \mathrm{L}/2$ [3].

As the next special case we can consider a so-called thermal symmetry (see Fig. 20). For example, two surfaces of a large hot plate of thickness L suspended vertically in air will be subjected to the same thermal conditions, and thus the temperature distribution in one half of the plate will be the same as that in the other half [3]. Hence, the heat transfer problem in the plate contains thermal symmetry at $x = \mathrm{L}/2$. We can express this situation by

$$\frac{\partial T(\mathrm{L}/2,t)}{\partial x}=0. \tag{29}$$

4.2.3 Convection boundary condition

Another type of boundary condition is called as Newton's condition. In fact, it is one of the most common conditions used in practice, since a heat transfer surfaces are in the environment together with a specified temperature. It is based on a surface energy balance, where heat conduction at a surface in specific selected direction is equal to the heat convection at that surface in the same direction. For 1D heat transfer through the plate of length L, we can express convection boundary condition in following way.

$$-k\frac{\partial T(0,t)}{\partial x}=htc_1\left[T_{\infty 1}-T(0,t)\right], \tag{30}$$

and

$$-k\frac{\partial T(\mathrm{L},t)}{\partial x}=htc_2\left[T(\mathrm{L},t)-T_{\infty 2}\right], \tag{31}$$

where htc_1 and htc_2 are the heat transfer coefficients and $T_{\infty 1}$, $T_{\infty 2}$ are the ambient temperatures on each side of the plate.

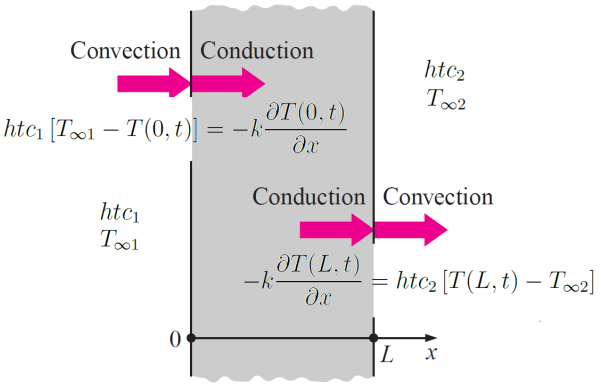

Figure 21: Convection boundary condition on both surfaces of a wall [3].

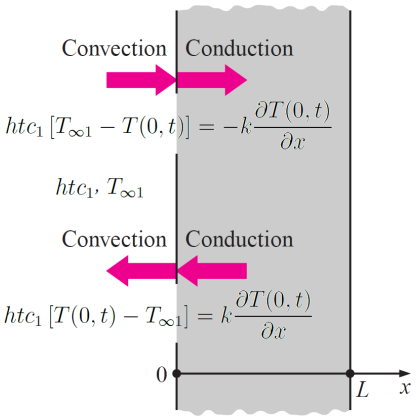

Figure 22: Direction of heat transfer at a boundary has no effect on boundary condition expression [3].

In the equation (30) and (31) we have selected positive x axis as direction of heat transfer (see Fig. 21). In that case, they remain the same and, in fact, the only equally applicable, when we choose an opposite direction. Both equations remains the same, where the only difference will be in the signs of convection and conduction term as shown in Figure 22. It is very pleasant to be able to choose both directions as direction of heat transfer because we often don't know the surface temperature and thus the heat transfer in advance. We should remind that surface has no thickness therefore no mass so it cannot store any energy. Thus, whole heat coming from one side must leave surface from the other side. So, basically convection boundary condition states that heat continuous to flow from body to the surroundings and vice versa.

4.2.4 Radiation boundary condition

Next introduced boundary condition is not in fact a typical one, but rather more interesting one. This boundary has its own usage in space and cryogenic applications. In this case, the heat transfer surface is surrounded by an evacuated space and thus, there is no convection heat transfer between a surface and the surrounding medium [3]. In this cases radiation is the only mechanism of heat transfer (see Fig. 23). Again using energy balance, radiation boundary condition is expressed as heat conduction at surface in selected direction is equal to radiation exchange at the surface in the same direction. On 1D wall of thickness L radiation boundary condition is:

$$-k\frac{\partial T(0,t)}{\partial x} = \varepsilon_1\sigma\left[T^4_{\text{surr},1} - \mathrm{T}(0,t)^4\right] \tag{32}$$

and

$$-k\frac{\partial T(\mathrm{L},t)}{\partial x} = \varepsilon_2\sigma\left[T(\mathrm{L},t)^4 - T^4_{\text{surr},2}\right] \tag{33}$$

where ε_1, ε_2 are emissivities of boundary surfaces σ is the Stefan-Boltzman constant and $T_{\text{surr},1}$ and $T_{\text{surr},2}$ are average temperatures of ambient of two sides of the wall.

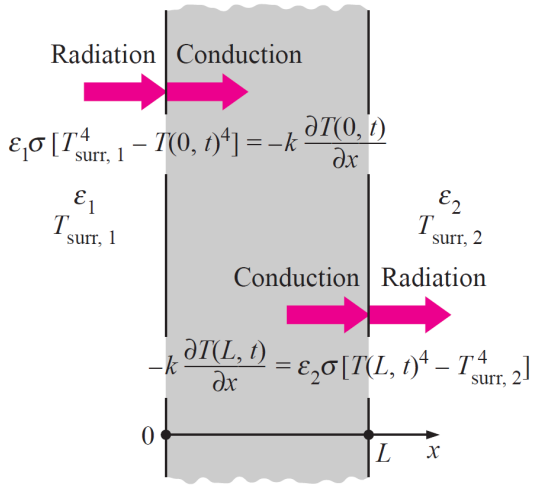

Figure 23: Radiation boundary condition on both sides of the wall [3].

We can see that the radiation boundary condition involves forth power of the temperature and so it is nonlinear therefore they are sometimes difficult to determine. In some applications where radiation is strongly suppressed by convection we can omit the radiation and avoid complications associated whit nonlinearity.

4.2.5 Interface boundary condition

The last boundary condition introduced here is usually used for bodies made of multiple materials. The solution of heat transfer through such a body requires a solution of heat transfer through its every layer. This problem will require some specific conditions on every interface of two materials. First one is that temperature at the contact area must be same for different materials and the second one is that interface cannot store any energy therefore heat flux on both sides must be same. The Figure 24 can be expressed as:

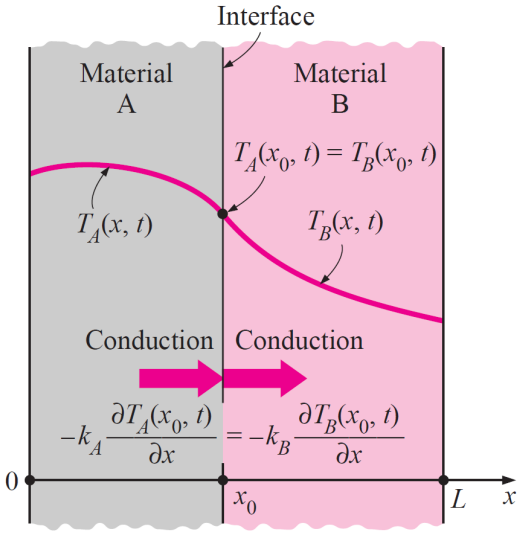

Figure 24: Boundary condition at the interface of two material with perfect contact [3].

$$T_A(x_0, t) = T_B(x_0, t) \tag{34}$$

and

$$-k_A\frac{\partial T_A(x_0, t)}{\partial x} = -k_B\frac{\partial T_B(x_0, t)}{\partial x}. \tag{35}$$

where k_A and k_A are thermal conductivities of two material.

4.3 Modeling of latent heat

There are two main approaches of modeling phase change considering the treatment of the phases interface. Methods based on interface capturing and methods based on interface tracking. In the interface capturing methods, the temperature distribution is solved as a major quantity and only little effort is devoted to the location and translation of the interface between the phases [6]. Usually in these methods we assume that the interface is a near isothermal surface corresponding to the phase change temperatures. On the other hand interface tracking methods also include techniques that explicitly track interface. They do it by use of finite number of points called markers which represent the interface and are precisely tracked. Even though interface tracking methods outperform interface capturing methods they are still less popular, probably due to limited information about efficiency, accuracy and requirements. Therefore we will consider only interface capturing methods especially the enthalpy method, the effective heat capacity method and the temperature recovery method. They are easy to implement in code, relatively fast to compute without the need for additional treatment, their mathematical formulation is relatively simple but they suffer from lower accuracy than interface tracking methods.

Modelling methods which use interface capturing are primarily focused on solution of heat transfer equation and obtaining temperature distribution. If we would need to determine interface position we could do that from temperature distribution using the assumption that interface lies somewhere between grid points where temperature is below and above phase change temperature.

4.3.1 Enthalpy method

Enthalpy method is one of the most frequently used methods for modeling heat transfer problems with phase change since it incorporates the term $\dot{Q}$, combining all internal heat sources. In this method we work with volume enthalpy $H(T)$ [J/m^3] which can be defined as a functional:

$$H(T) = \int_0^T \left[\rho(\xi)c(\xi) - \rho(\xi)L\frac{\partial f_s}{\partial T}\right] \mathrm{d}\xi. \tag{36}$$

From where we can derive:

$$H(T) = \int_0^T \rho(\xi)c(\xi)\mathrm{d}\xi + \rho(T)\left(1 - f_s\right)L. \tag{37}$$

For each phase the volume enthalpy will be:

$$H = \begin{cases} \rho(T)c(T)T, & T \leq T_S \\ \rho(T)\left(c(T)T + \left(1 - f_s\right)L\right), & T_S < T < T_L \\ \rho(T)(c(T)T + L), & T \geq T_L \end{cases} \tag{38}$$

where T_S denotes solid temperature, where the whole volume is in solid phase and T_L expresses liquid temperature, where the material is in liquid phase. So in the equations (15) - (18) we will substitute enthalpy and get:

$$\frac{\partial H}{\partial t} = k(T)(\Delta T) + v_z\frac{\partial H}{\partial z}, \tag{39}$$

$$\frac{\partial H}{\partial t} = k(T)(\Delta T) + v_z \frac{1}{r}\frac{\partial H}{\partial \varphi}. \tag{40}$$

In this method enthalpy is the main variable and equation (39) or (40) is considered to be mathematically complete, therefore they can be numerically solved by an appropriate computational method. Enthalpy based formulation of the heat transfer equation contains two unknowns. These two unknowns are coupled with the equation (36) and computational solution is carried out in two steps. First, enthalpy is determined from equations (39), (40) and then temperature from (38), where a typical enthalpy temperature relation can be seen in Figure 25. This two-step technique makes the numerical procedure more demanding [6]. We will discuss numerical solution and implementation later in the text.

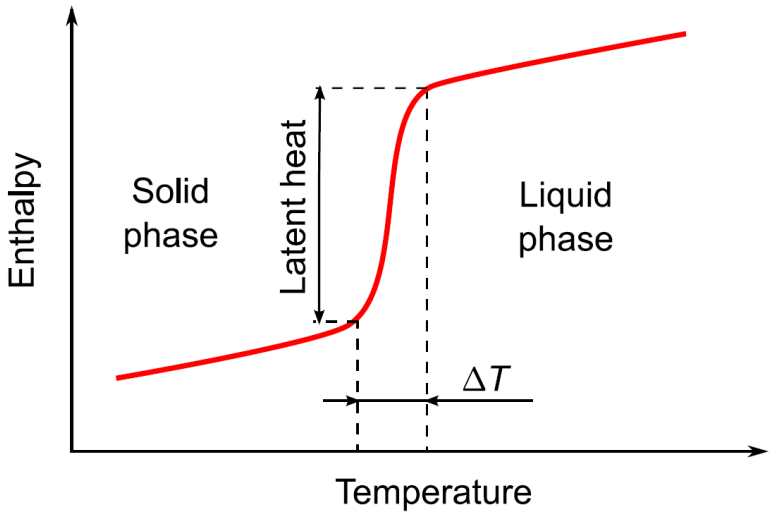

Figure 25: Typical temperature-enthalpy relationship for the non-isothermal phase change. [6].

4.3.2 Effective heat capacity method

Effective heat capacity method, in some literature also called apparent heat capacity, is another interface capturing method where latent heat is included in $c_{eff}(T)$ [J/m^{3}K]. We can define it as:

$$c_{eff}(T) = \frac{\partial H}{\partial T} = \rho(T)c(T) - \rho(T)L\frac{\partial f_s}{\partial T}. \tag{41}$$

If we assume linear release of the latent heat, than effective heat capacity for each phase results in expression:

$$c_{eff} = \begin{cases} c(T)\rho(T), & T < T_S \\ c(T)\rho(T) + \frac{L\rho(T)}{(T_L - T_S)}, & T_S \leq T \leq T_L \\ c(T)\rho(T). & T > T_L \end{cases} \tag{42}$$

We can rewrite (17), (18) with effective heat capacity and we will obtain:

$$c_{eff}(T)\frac{\partial T}{\partial t} = k(T)(\Delta T) + c_{eff}(T)v_z\frac{\partial T}{\partial z}, \tag{43}$$

$$c_{eff}(T)\frac{\partial T}{\partial t} = k(T)(\Delta T) + c_{eff}(T)v_z\frac{1}{r}\frac{\partial T}{\partial \varphi}. \tag{44}$$

Effective heat capacity method differs from enthalpy method in a way that the primary variable is directly computed from (43), (44) which eliminates variations caused by two steps in the enthalpy method. Moreover we can use implicit Euleur method which guarantees stability for arbitrary time step and shortens the total computational time. Figure 26 depicts characteristic bell shaped temperature-effective heat capacity relation.

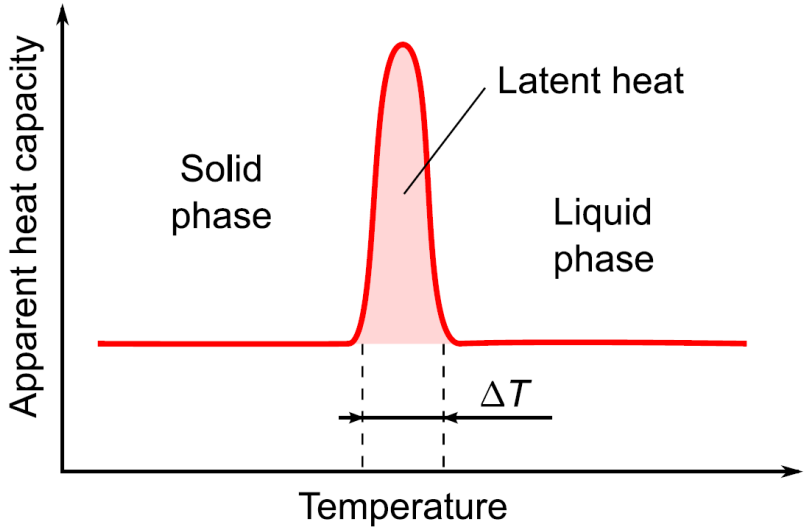

Figure 26: Characteristic bell-shaped effective heat capacity [6].

On the other hand effective heat capacity method has some drawbacks. The main one is that it is hard to ensure energy conservation. What can happen is, that if we compute node temperature in the first time step and temperature of the same node in the next time step, we can completely skip latent heat addition if the temperature difference is too big. Therefore effective heat capacity method needs some correction for example like the one used in [12]:

$$c_{eff} = \begin{cases} \frac{(H_2-H_1)}{(T_2-T_1)}, & (T_2-T_1) \geq \varepsilon \\ c_{eff}\,(T_2)\,, & (T_2-T_1) < \varepsilon \end{cases} \tag{45}$$

where ε is a small temperature difference in node (for example $\varepsilon \leq 0.1$ K), $H_2 - H_1$ denotes enthalpy difference in two adjacent time steps T_2, T_1. We will discuss the correction later in the text.

4.3.3 Temperature recovery method

Another useful variant of enthalpy techniques is temperature recovery method. In this method, the temperature at which phase change occurs is computed in two steps. In the first step, the temperature is calculated with absence of latent heat. In the second step temperature is set back to the phase change temperature and the equivalent amount of heat is added to the enthalpy budget for a node. We can compute released latent heat as a function of corresponding increment of solid segment over a time step. Once the

enthalpy budget equals the latent heat for the volume associated with that node, the temperature is allowed to fall according to the heat diffusion [12]. Scheme of the principle of the temperature recovery method can be seen in Figure below (27).

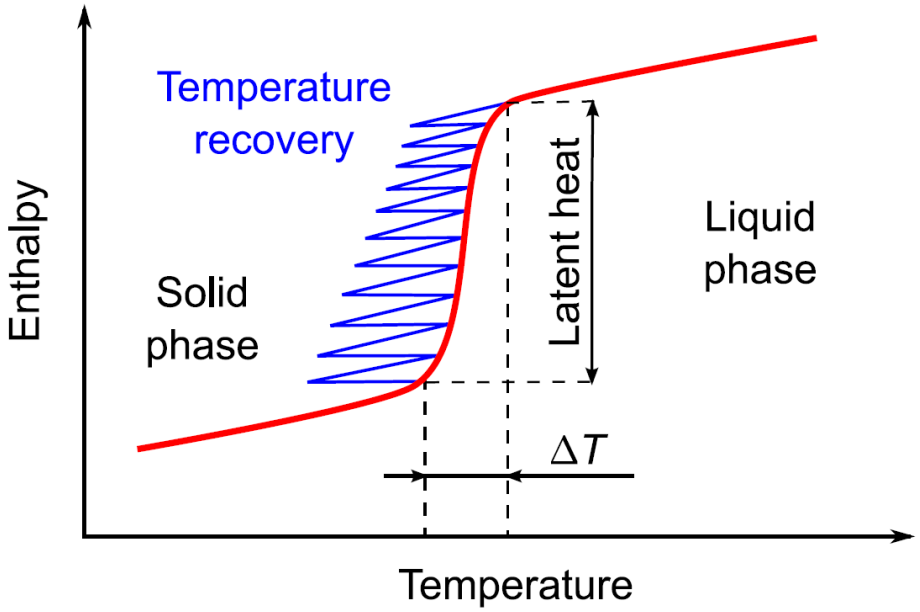

Figure 27: Principle of the temperature recovery method [6].

So with this method,heat transfer model:

$$\rho(T)c(T)\frac{\partial T}{\partial t} = k(T)\Delta T, \tag{46}$$

is corrected according to:

$$T = \begin{cases} T, & T < T_S \\ T_L - (H_2 - H_1)\,(T_2 - T_1)\,\frac{1}{L}, & T_S \leq T \leq T_L \\ T, & T > T_L \end{cases} \tag{47}$$

where again $H_2 - H_1$ expresses enthalpy difference of the two adjacent time steps T_2, T_1 and T_S, T_L is solid and liquid temperature.

Main advantage of the temperature recovery method is that the conservation of energy is ensured, it is easy to implement and computationally not very demanding. Another big advantage of this approach is the fact that it decouples enthalpy, temperature and phase transformation calculations, which is used for solidification models where enthalpy-temperature relation is not known beforehand. As a disadvantage can be seen its sensitivity to the size of the time step and that errors in the approximation are larger in neighborhood of the mushy zone than in the single phase area.

5 Numerical model

Numerical analysis is in fact a very useful tool of mathematics, particularly to problems of unsolvable matter. In other words, if we are not able to get analytical solution, we use an appropriate numerical method. There are two main categories of numerical approaches. Namely, mesh and mesh free methods.

Mesh methods have defined points that create mesh structure, while mesh free are based on interaction of each node with all its neighbors. As a consequence, original extensive properties such as mass or kinetic energy are no longer assigned to mesh elements, but rather to single nodes.

One of the popular mesh free methods is moving particle method, which allows better local refinement of the mesh. The most common mesh methods are the finite difference method, the finite element method, the boundary element method, and the energy balance (or control volume) method. Every method has some advantages and disadvantages for different applications, but we will focus more on the finite difference method. Following text was inspired by [3], [7],[9], [15], [19].

5.1 Finite difference method

Finite difference method is one of the oldest and the easiest methods to apply to simple geometry. This method is based on the principle of replacing differential equations by algebraic ones. It is done by replacing derivations by finite differences, where also the name of the method comes from. We can approximate derivations by use of Taylor series expansion or by polynomial fitting. First derivative of a function $f(x)$ at a point is equivalent to the slope of a line tangent to the curve at that point and is defined as [3]:

$$\frac{df(x)}{dx} = \lim_{\Delta x \to 0} \frac{\Delta f}{\Delta x} = \lim_{\Delta x \to 0} \frac{f(x + \Delta x) - f(x)}{\Delta x}, \tag{48}$$

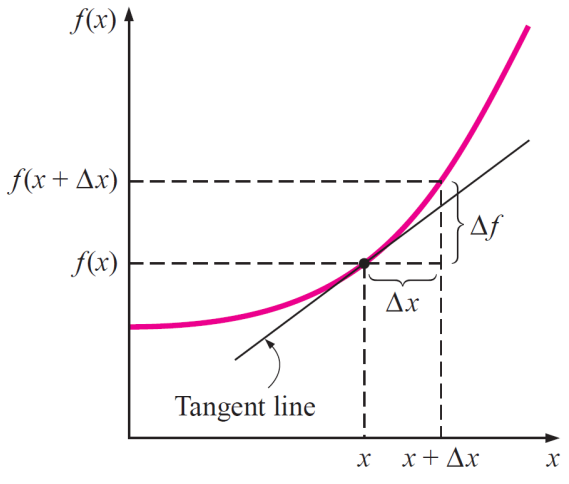

Figure 28: The derivative of a function at a point represents the slope of the function at that point [3].

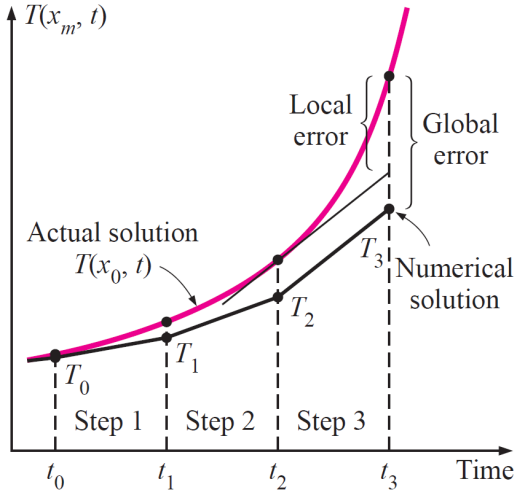

Figure 29: Local and global discretization errors of the finite difference method at the third time step at a specified nodal point [3].

where $\frac{\Delta f}{\Delta x}$ is the ratio which denotes increment of the function relative to Δx. So for Δx

sufficiently small we can write:

$$\frac{df(x)}{dx} \cong \frac{f(x+\Delta x)-f(x)}{\Delta x}. \tag{49}$$

We can obtain the same equation by writing Taylor expansion of a function f about a point x and neglecting all terms of the expansion except for the first two:

$$f(x+\Delta x) = f(x) + \Delta x \frac{df(x)}{dx} + \frac{1}{2}\Delta x^2 \frac{d^2 f(x)}{dx^2} + \cdots . \tag{50}$$

Because in our problem second derivative of a temperature in a specific direction occurs, we need to introduce the second derivative. Firstly we need to show the first derivative:

$$\left.\frac{\partial T}{\partial x}\right|_{i-\frac{1}{2}} \cong \frac{T_i - T_{i-1}}{\Delta x_{i-1}}, \quad \left.\frac{\partial T}{\partial x}\right|_{i+\frac{1}{2}} \cong \frac{T_{i+1} - T_i}{\Delta x_i}. \tag{51}$$

And now the second derivative:

$$\left.\frac{\partial^2 T}{\partial x^2}\right|_i \cong \frac{\left.\frac{\partial T}{\partial x}\right|_{i+\frac{1}{2}} - \left.\frac{\partial T}{\partial x}\right|_{i-\frac{1}{2}}}{\frac{\Delta x_i + \Delta x_{i-1}}{2}} = \frac{\frac{T_{i+1}-T_i}{\Delta x_i} - \frac{T_i - T_{i-1}}{\Delta x_{i-1}}}{\frac{\Delta x_i + \Delta x_{i-1}}{2}}. \tag{52}$$

In case of equidistant distribution of points $\Delta x = \Delta x_i = \Delta x_{i-1}$, second derivative can be approximated by second central difference:

$$\left.\frac{\partial^2 T}{\partial x^2}\right|_i \cong \frac{T_{i-1} - 2T_i + T_{i+1}}{(\Delta x)^2}. \tag{53}$$

Time discretization of the temperature looks like:

$$\frac{\partial T}{\partial t} \cong \frac{T_{i,j}^{n+1} - T_{i,j}^{n}}{\Delta t}, \tag{54}$$

where n denotes actual time step and $n+1$ following time step.

5.1.1 Accuracy and controlling of numerical error

Accuracy is without a doubt connected to the errors occurring in numerical computations. When we compare our numerical results with exact solutions we may or may not have sufficiently approximate numerical solutions. The difference between numerical and exact solution is called error and it is generated primarily by discretization error and round-off error.

Discretization error also called truncation or formulation error occurs when we replace derivatives by finite differences in each step or the actual temperature distribution between two adjacent nodes by a straight line. When we look at Figure 29, we can see that in the beginning numerical and exact solutions coincides as expected, but with increasing time numerical solution deviates more and more. The difference between the two solutions in t_i and t_{i+1} is called local discretization error. One can predict that the situation will only get worse after n time steps since the numerical solution in t_{i+1} is computed from previous time step which already has some numerical error. The accumulation of local errors after n time steps is called global discretization error. Note that local and global

discretization errors are identical for the first time step [3]. Global discretization error usually increases with increasing number of steps, but the opposite may occur when the solution function changes direction frequently, giving rise to local discretization errors of opposite signs, which tend to cancel each other out [3].

Local discretization error gives us the first idea about accuracy of the method, however as we stated before, after each time step the error accumulates, so what we are really looking for, is the global discretization error. When we look at equation (50) the first neglected term is $(\Delta x)^2$, so the approximation error of one step is equal to $(\Delta x)^2$. However cumulative error after M steps on distance L is adequate to Δx since $M\Delta x^2 = (L/\Delta x)\Delta x^2 = L\Delta x$. Therefore smaller Δx means smaller global error and thus better approximation.

Round-off error is the error which occurs due to limited number of digits per number in computer. Typically computers use 7 digits per number, which is called single precision, however we may perform calculations using 15 digits, referred to as double precision. But we have to keep in mind that double precision uses more memory and requires more computational time. This error is very hard to predict because it is random. It depends on the number of calculations, the method of rounding off, the type of computer, and even the sequence of calculations [3]. It is proportional to the number of calculations executed during computation of the solution.

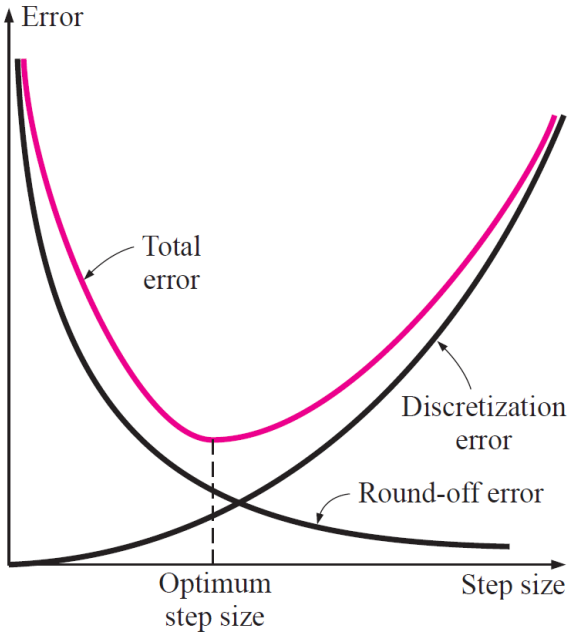

Figure 30: As the mesh or time step size decreases, the discretization error decreases but the round-off error increases.[3].

Total error present in the numerical method is sum of discretization error, which decreases with decreasing step size and round-off error, which increases with decreasing step size. Therefore reducing the step size in order to achieve better solution form point of view of discretization may result in complete opposite effect. So we should be always careful not to let round-off error get out of "control" by avoiding working with too small or too large numbers.

In practice most of the times we don't know the exact solution, thus we cannot fully determine the magnitude of error present in numerical method. Even knowing global discretization error is meaningless without a good estimate of round-off error. Therefore to assess the accuracy of the results obtained by numerical method we should:

1. Start the calculation with reasonable mesh size Δx based on our experience and then repeat the calculation with $\frac{\Delta x}{2}$. When results do not differ from previous ones in any significant way, we can conclude that the discretization error is at an acceptable level. If the difference between the results is bigger than we can accept, we continue halving mesh size until the results are sufficient.
2. Calculate the problem with double precision holding the mesh size constant. If changes are not significant we may conclude that the round-off error is not a problem, but if they are too large we can try to increase mesh size and thus reduce the number of calculations, or to change the order of computations. With increasing mesh size we have to find suitable compromise for both errors.

5.1.2 Stability criterion for explicit method

Explicit method is easier to implement but it has a major disadvantage compared to the implicit method. Time step Δt is limited by its size, method is not unconditionally stable. Big time step may cause oscillations or even divergence of the method. To prevent this from happening, stability criterion must be satisfied. For computation of all temperatures in the next time step at all nodes i, j we can write:

$$\begin{aligned} T_{i,j}^{n+1} &= a_{i,j} T_{i,j}^{n} + \dots \\ T_{i+1,j}^{n+1} &= a_{i+1,j} T_{i+1,j}^{n} + \dots \\ &\vdots \\ T_{i,j+1}^{n+1} &= a_{i,j+1} T_{i,j+1}^{n} + \dots \\ &\vdots \\ a_{i,j} &\geq 0. \qquad \forall i, j \end{aligned} \tag{55}$$

For stability condition to be satisfied, all coefficients $a_{i,j}$ before $T_{i,j}^{n}$ must be greater or equal to zero for all nodes, which also satisfies second law of thermodynamic.

For 2D case of heat transfer inside of a body, stability criterion will be obtained from:

$$T_{i,j}^{n+1} = \left(1 - \frac{2\Delta t k}{(\Delta x)^2 \rho c} - \frac{2\Delta t k}{(\Delta y)^2 \rho c}\right) T_{i,j}^{n} + \dots \tag{56}$$

where form equation (55) we get:

$$\begin{aligned} \left(1 - \frac{2\Delta t k}{(\Delta x)^2 \rho c} - \frac{2\Delta t k}{(\Delta y)^2 \rho c}\right) &\geq 0, \\ 1 &\geq \Delta t \left(\frac{2k}{(\Delta x)^2 \rho c} + \frac{2k}{(\Delta y)^2 \rho c}\right), \\ \Delta t &\leq \frac{\rho c (\Delta x)^2 (\Delta y)^2}{2k(\Delta y)^2 + 2k(\Delta x)^2}, \end{aligned} \tag{57}$$

so for Δt_{inside} we have:

$$\Delta t_{\text{inside}} \leq \frac{(\Delta x)^2 (\Delta y)^2}{2\alpha(\Delta y)^2 + 2\alpha(\Delta x)^2}, \tag{58}$$

where $\alpha = \frac{k}{c\rho}\,[\mathrm{m}^2/\mathrm{s}]$ is thermal diffusivity. Situation gets even more complicated because thermophysical properties depend on temperature and we can have non-equidistant mesh. Thus computation of time step for every iteration is unnecessarily complicated. Usually the worst case scenario is utilized for time step which gives us:

$$\Delta t_{\text{inside}} \leq \frac{\min\limits_{T}\{\rho(T)c(T)\}\min\limits_{i}\{(\Delta x)^2\}\min\limits_{j}\{(\Delta y)^2\}}{2\max\limits_{T}\{k(T)\}\max\limits_{j}\{(\Delta y)^2\} + 2\max\limits_{T}\{k(T)\}\max\limits_{i}\{(\Delta x)^2\}} \tag{59}$$

Criteria for 1D or 3D are analogical. However criterion for boundary nodes depends on boundary condition. For Dirichlet or Neumann condition criterion stays the same, but for radiation or Newton condition for example, criterion will also become the function of heat transfer coefficient in a particular direction:

$$\Delta t_{\text{boundary}} \leq \frac{1}{\frac{2htc}{c\rho\Delta x} + \frac{2k}{c\rho(\Delta x)^2} + \frac{2k}{c\rho(\Delta y)^2}} \tag{60}$$

Note that the node with the strictest criterion is the corner point. With all this in mind we can set the final criterion, which will be the smallest time step of all possible ones:

$$\Delta t = \min\left\{\Delta t_{\text{inside}}, \Delta t_{\text{boundary}}\right\}. \tag{61}$$

5.2 2D Slice model

In this thesis we are using 2D slice model rather than fully 3D model to simulate continuous casting of steel.

Slice models were successfully implemented by Lally [9], Šarler [15], Klimeš [7], Zhang [19] etc. Lally showed that thermal profiles computed by slice models agree with those predicted by 3D models. He also found that they significantly increase efficiency and reduce computational requirements. For example usage of 2D slice model for several finite difference methods resulted in a reduction of computation time from 338 minutes to just 2 minutes without sacrificing accuracy. Since they are so fast, they can be used for fast optimization or online simulations. Even Šarler suggested slice models for heat transfer, but he also pointed out their significant drawbacks in predicting realistic turbulent fluid flow effects [15].

Principle is similar to 3D model with radial casting, but in 2D slice model casting process occurs in the horizontal direction. We neglect all interactions in the casting direction and take into account only those perpendicular to the casting in form of a traveling slice. Is was well reported that this assumption leads to only small inaccuracies since interactions perpendicular to the casting speed are way more significant.

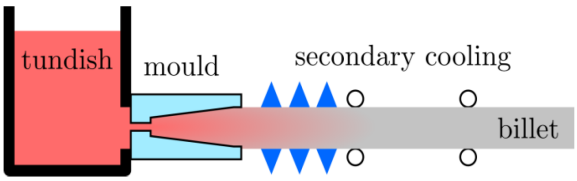

Figure 31: Schematic of horizontal continuous casting [7].

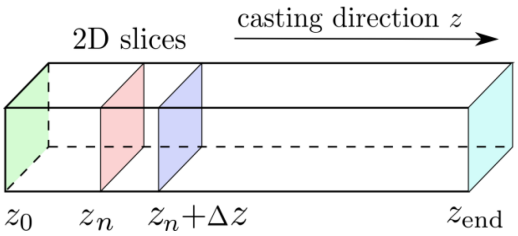

Figure 32: Slice model principle [7].

Temperature field of the slice is computed from known time dependent boundary conditions, where slice time is connected to the position in the strand. Since we can neglect all interactions in the casting direction, temperature fields at a given coordinate z depend only on slice history, including its cooling intensity. To calculate the cooling intensity of the slice as a function of time, a connection between the z coordinate of the casting machine and the slice history t is needed, which in general is [15]:

$$z(t) = \int_{t_{\text{start}}}^{t} v_z\left(\xi\right) \cdot d\xi + z_{\text{start}}, \tag{62}$$

where t_{start} is the initial time of the slice and v_z is a casting speed. We may obtain simple connection between z coordinate and slice history, when casting speed and other parameters are steady:

$$t(z) = t_{\text{start}} + \frac{z - z_{\text{start}}}{v_z}. \tag{63}$$

After the computation, when slice arrives at the end, 3D model can be reconstructed as a temperature history of 2D slices.

5.3 Numerical formulation of the methods

Further we will show how to discretize partial differential equation (16) as well as boundary conditions. Since we are working with slice model and assume equidistant mesh, (16) we will get even simpler problem discretized as follows:

$$\rho_{i,j} c_{i,j} \frac{T_{i,j}^{n+1} - T_{i,j}^{n}}{\Delta t} = k_{i,j} \left(\frac{T_{i-1,j} - 2T_{i,j} + T_{i+1,j}}{(\Delta x)^2} + \frac{T_{i,j-1} - 2T_{i,j} + T_{i,j+1}}{(\Delta y)^2} \right) + \dot{Q} \tag{64}$$

To keep the equation more neat we ignored dependence on temperature $\left(T_{i,j}^{n}\right)$ for parameters where the dependency is obvious.

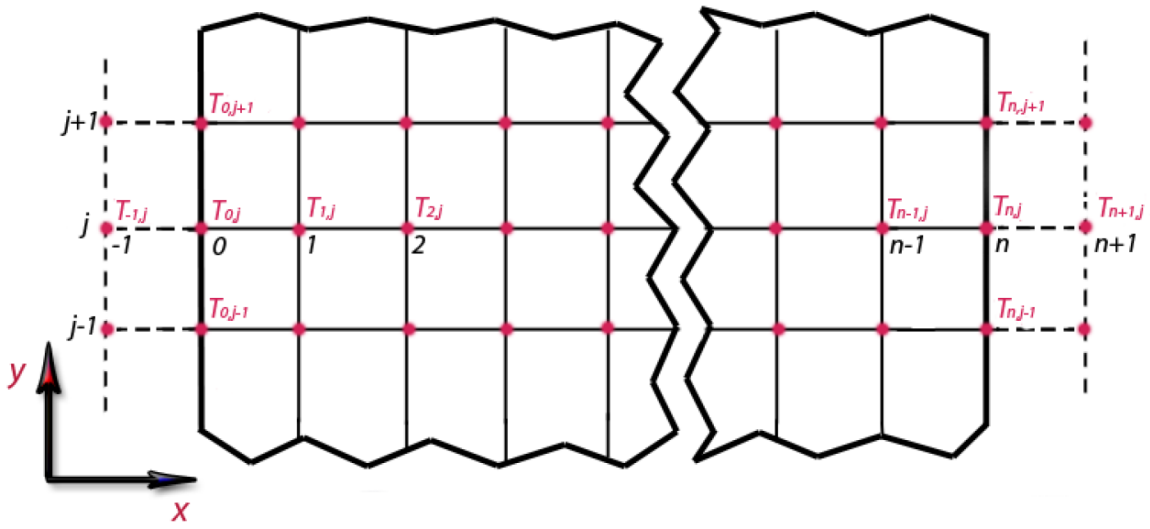

Figure 33: Example of discretization of edge nodes [11].

Equation (64) can only be used for internal nodes, because for boundary nodes $i = 0$ and $i = n$, where n denotes the number of nodes in x direction, we need to know values of nodes $i = -1$ and $i = n + 1$ which we don't have right now (see Fig. 33). Similarly for j nodes in y direction. Temperatures in imaginary nodes $i = -1$ and $i = n + 1$ can be obtained from boundary conditions. To keep the text simple and well-arranged, we will show to compute edge node $i = -1$, because for other imaginary edge nodes it is analogical. To obtain its value we use boundary conditions:

1. Dirichlet boundary condition:

$$T^n_{0,j} = T_{\text{surf}}. \tag{65}$$

2. Radiation boundary condition:

$$\begin{aligned} -k\frac{T^n_{-1,j} - T^n_{1,j}}{2\Delta x} &= \epsilon\sigma\left(\left(T^n_{0,j}\right)^4 - T^4_\infty\right) \Longrightarrow \\ \Longrightarrow T^n_{-1,j} &= -\frac{\epsilon\sigma\left(\left(T^n_{0,j}\right)^4 - T^4_\infty\right)2\Delta x}{k} + T^n_{1,j}. \end{aligned} \tag{66}$$

3. Neumann boundary condition utilizes first central difference:

$$-k\frac{T^n_{-1,j} - T^n_{1,j}}{2\Delta x} = \dot{q} \Longrightarrow T^n_{-1,j} = -\frac{2\Delta x\dot{q}}{k} + T^n_{1,j}. \tag{67}$$

- For special case of heat flux boundary, when edge is insulated, we get:

$$-k\frac{T^n_{-1,j} - T^n_{1,j}}{2\Delta x} = 0 \Longrightarrow T^n_{-1,j} = T^n_{1,j}. \tag{68}$$

4. Newton boundary condition:

$$\begin{aligned} -k\frac{T^n_{-1,j} - T^n_{1,j}}{2\Delta x} &= htc\left(T^n_{0,j} - T_\infty\right) \Longrightarrow \\ \Longrightarrow T^n_{-1,j} &= -\frac{htc\left(T^n_{0,j} - T_\infty\right)2\Delta x}{k} + T^n_{1,j}. \end{aligned} \tag{69}$$

- Combined convection radiation contition:

$$\begin{aligned} -k\frac{T^n_{-1,j}-T^n_{1,j}}{2\Delta x} &= htc\left(T^n_{0,j}-T_\infty\right)+\sigma\varepsilon\left(\left(T^n_{0,j}\right)^4-T^4_\infty\right)\Longrightarrow \\ \Longrightarrow T^n_{-1,j} &= -\frac{2\Delta x\left[htc\left(T^n_{0,j}-T_\infty\right)+\sigma\varepsilon\left(\left(T^n_{0,j}\right)^4-T^4_\infty\right)\right]}{k}+T^n_{1,j}. \end{aligned} \tag{70}$$

When we know the values of imaginary nodes, we can execute (64) on boundary nodes $i = 0$ as well. Note that in all of the above equations k and htc depends on surface temperature, $k\left(T^n_{0,j}\right)$, $htc\left(T^n_{0,j}\right)$.

6 Implementation of numerical model

In this section we will show discretization of the methods modeling latent heat and describe how they were implemented. To keep the equations more neat, we will omit the explicit notation of dependency on temperature in time step n, for all thermophysical properties, for example $k_{i,j}\left(T_{i,j}^{n}\right)$ will be denoted as $k_{i,j}$, unless it is specified otherwise.

6.1 Numerical formulation of enthalpy method

Modeling of latent heat via enthalpy method is thanks to experimental and IDS program data very pleasant to implement. We start , as in all methods, by setting initial temperature for the whole slice:

$$T_{i,j}^{n=0} = T_{\text{casting}} \quad \forall i,j \tag{71}$$

Subsequently depending on the boundary condition we recompute edge temperatures. Knowing when to use what type of boundary is essential for good prediction of the continuous casting behavior. Since we have the relation between time, casting velocity and z position (62),(63), this doesn't have to bother us. We solve simplified, thanks to the slice model, equation (39) for every node where its numerical discretization looks:

$$\begin{aligned} \frac{H_{i,j}^{n+1} - H_{i,j}^{n}}{\Delta t} &= k_{i,j}\left(\frac{T_{i-1,j} - 2T_{i,j} + T_{i+1,j}}{(\Delta x)^2} + \frac{T_{i,j-1} - 2T_{i,j} + T_{i,j+1}}{(\Delta y)^2}\right) \\ H_{i,j}^{n+1} &= H_{i,j} + k_{i,j}\Delta t\left(\frac{T_{i-1,j} - 2T_{i,j} + T_{i+1,j}}{(\Delta x)^2} + \frac{T_{i,j-1} - 2T_{i,j} + T_{i,j+1}}{(\Delta y)^2}\right) \end{aligned} \tag{72}$$

Now we convert enthalpy back to temperature by known enthalpy-temperature relation (see Figure 34) for specific steel.

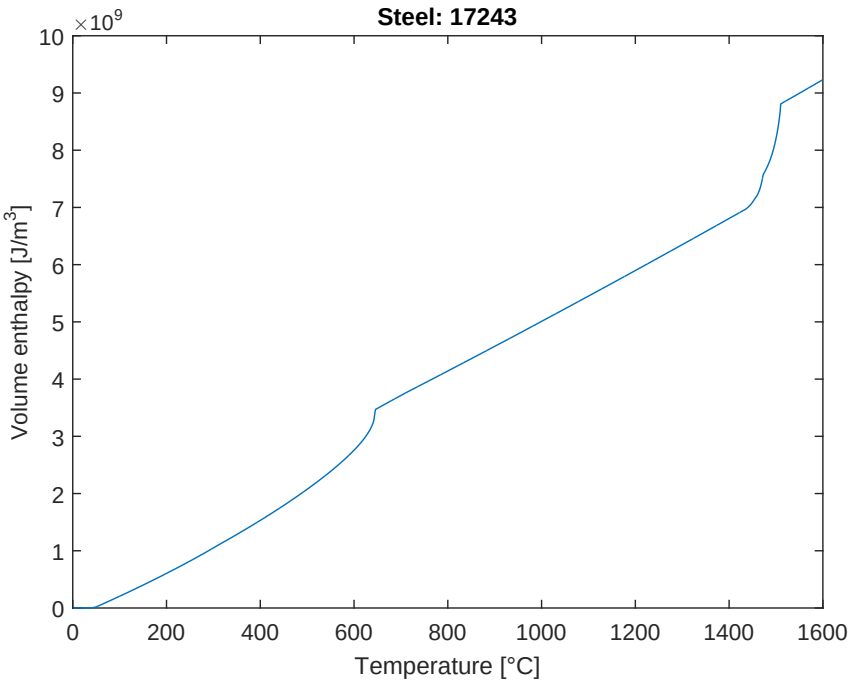

Figure 34: Known enthalpy-temperature relation for steel 17243.

Since enthalpy is a non-decreasing function, we have temperature and enthalpy vectors arranged from lowest to highest value. Therefore we can apply binary search algorithm for finding position i of the computed enthalpy H, thus the corresponding temperature. The algorithm works as follows:

1. Set $lower = 1$ and $upper = n$.
2. Check if $upper < lower$ than break with unsuccessful result, else set $i = \frac{upper+lower}{2}$.
3. Now compare computed H with enthalpy on i-th position, H_i. If $H < H_i$ than go to 4. If $H > H_i$ than go to 5. If $H = H_i$ than break with successful result and assign temperature on i-th position to computed enthalpy H.
4. Set $upper = i - 1$ and return to 2.
5. Set $lower = i + 1$ and return to 2.

Disadvantage of the whole approach is frequent using of binary search algorithm. We have to call it not only for every time step, but also for every node. This consumes the most of the computing time. One way of speeding up this process is to parallelize it on multiple processors.

After we obtain all temperatures $T_{i,j}^{n+1}$, we start again repeating the entire process for another time step.

6.2 Numerical formulation of effective heat capacity method

Although effective heat capacity is straightforward from the viewpoint of coding, because we work directly with temperature and there is no need for converting, it might get a bit trickier when we implement correction. Correction is necessary because of large numerical errors occurring due to reasons mentioned in (4.3.2).

Since we know that $c_{eff} = \frac{\partial H}{\partial T}$, we compute the c_{eff} from the known enthalpy beforehand.

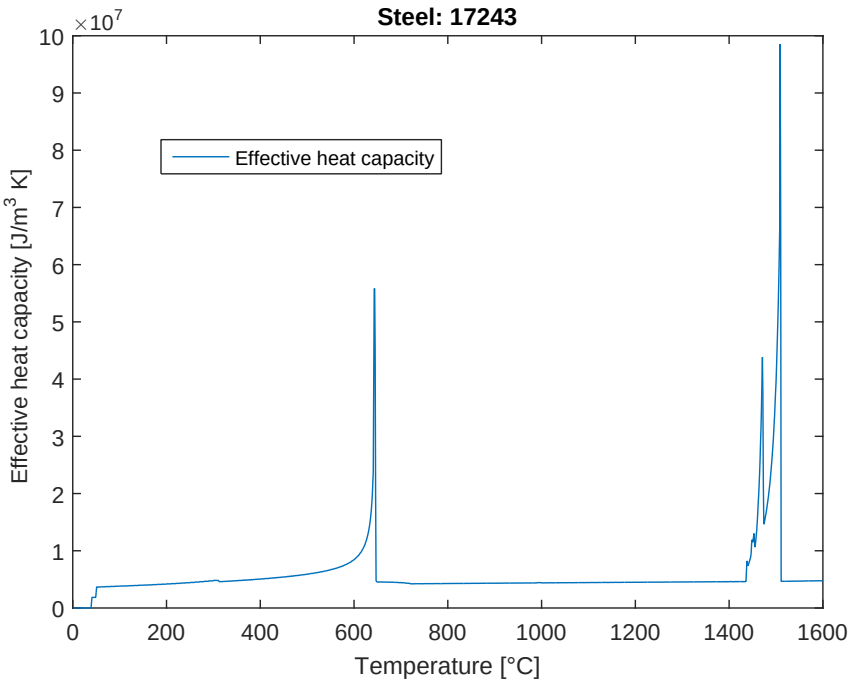

Figure 35: Effective heat capacity for steel 17243.

Again we calculate boundary temperatures using edge conditions and the process to compute temperatures in the following time step utilizing effective heat capacity is discretized as follows:

$$\begin{aligned} c_{eff_{i,j}} \frac{T_{i,j}^{n+1} - T_{i,j}^{n}}{\Delta t} &= k_{i,j} \left(\frac{T_{i-1,j} - 2T_{i,j} + T_{i+1,j}}{(\Delta x)^2} + \frac{T_{i,j-1} - 2T_{i,j} + T_{i,j+1}}{(\Delta y)^2} \right) \\ T_{i,j}^{n+1} &= \frac{k_{i,j}\Delta t}{c_{eff_{i,j}}} \left(\frac{T_{i-1,j} - 2T_{i,j} + T_{i+1,j}}{(\Delta x)^2} + \frac{T_{i,j-1} - 2T_{i,j} + T_{i,j+1}}{(\Delta y)^2} \right) + T_{i,j}^{n} \end{aligned} \tag{73}$$

Now we have to correct the results. First we will show correction proposed by Chia Liu and Sun Chao [10]. They suggested to correct specific heat as follows:

$$c_{eff_{i,j}} = \begin{cases} c_1 & T_\mathrm{f} - \Delta T > T^{n+1} \text{ and } T_\mathrm{f} - \Delta T > T^{n} \\ c_2 & T_\mathrm{f} - \Delta T > T^{n+1} \text{ and } T_\mathrm{f} + \Delta T \geq T^{n} \geq T_\mathrm{f} - \Delta T \\ c_3 & T_\mathrm{f} - \Delta T > T^{n+1} \text{ and } T_\mathrm{f} + \Delta T < T^{n} \\ c_4 & T_\mathrm{f} - \Delta T \leq T^{n+1} \leq T_\mathrm{f} + \Delta T \text{ and } T_\mathrm{f} - \Delta T \leq T^{n} \leq T_\mathrm{f} + \Delta T \\ c_5 & T_\mathrm{f} - \Delta T \leq T^{n+1} \leq T_\mathrm{f} + \Delta T \text{ and } T_\mathrm{f} + \Delta T < T^{n} \\ c_6 & T_\mathrm{f} + \Delta T < T^{n+1} \text{ and } T_\mathrm{f} + \Delta T < T^{n} \end{cases} \tag{74}$$

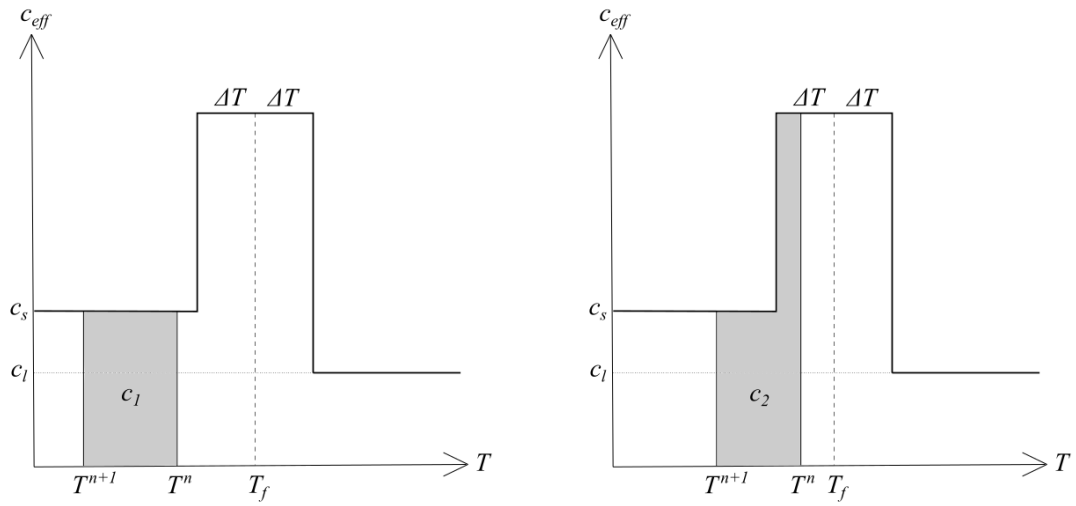

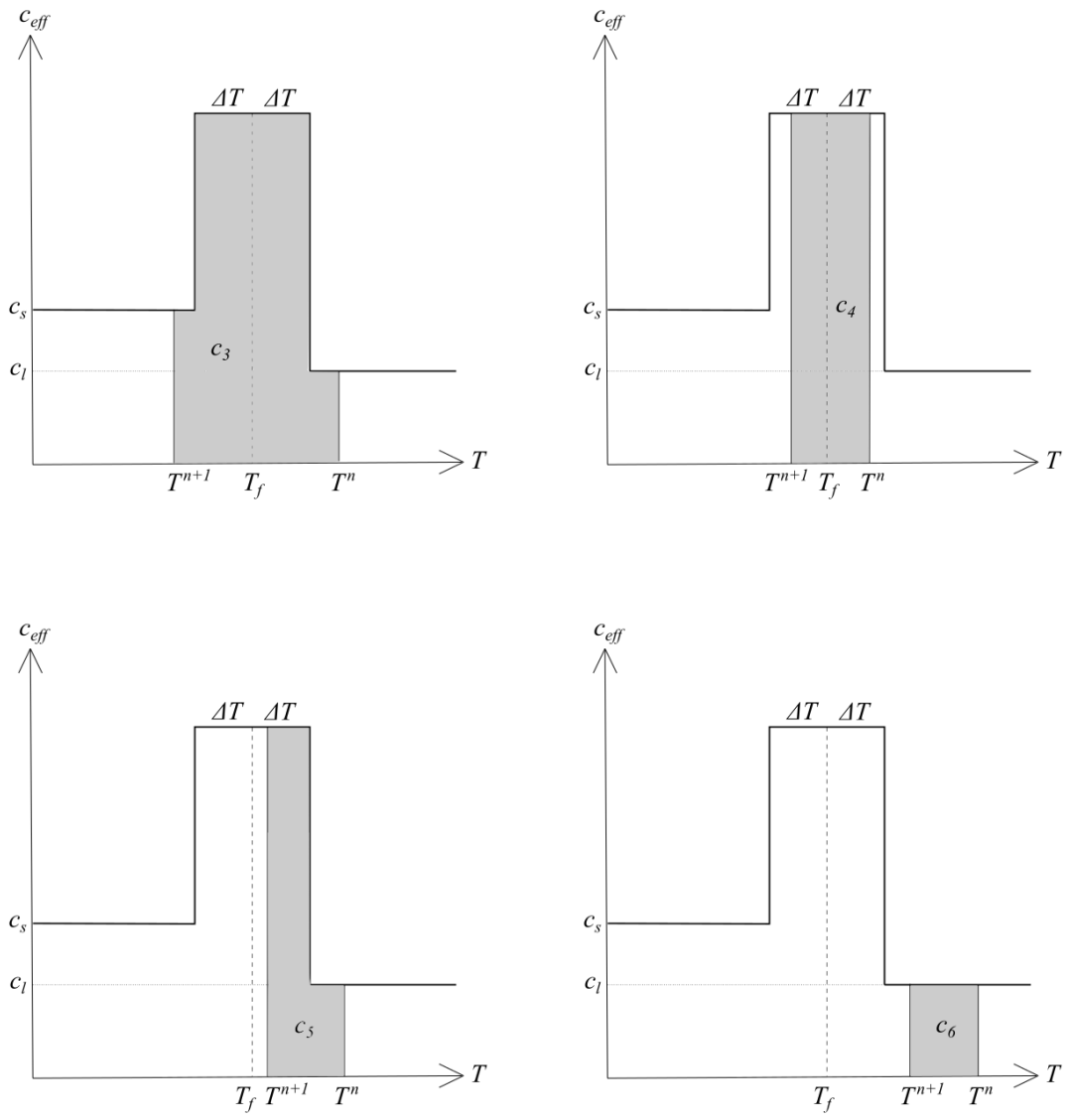

Figure 38: Areas of equation (74) depicted more clearly.

where

$$
\begin{aligned}
c_1 &= c_s \\
c_2 &= c_s + \frac{(c_4 - c_s)\,(T^n - T_{\mathrm{f}} + \Delta T)}{T^n - T^{n+1}} \\
c_3 &= c_s + \frac{2\Delta T\,(c_4 - c_s) - (c_s - c_l)\,(T^n - T_{\mathrm{f}} - \Delta T)}{T^n - T^{n+1}} \\
c_4 &= \frac{1}{2}\left(\frac{L}{\Delta T} + c_l + c_s\right) \\
c_5 &= c_4 - \frac{(c_4 - c_l)\,(T^n - T_{\mathrm{f}} - \Delta T)}{T^n - T^{n+1}} \\
c_6 &= c_l
\end{aligned}
\tag{75}
$$

where $T_{\mathrm{f}} = \frac{T_L + T_S}{2}$ is temperature as depicted in Figure 38; T_L, T_S are liquid and solid temperatures; $\Delta T = T_L - T_{\mathrm{f}}$; c_s, c_l are effective heat capacities for solid, liquid phase and

L denotes latent heat.

Another way of correcting effective heat capacity method was shown in [12] equation, (45), which written numerically is:

$$c_{eff_{i,j}} = \begin{cases} \frac{\left(H_{i,j}^{n+1} - H_{i,j}^{n}\right)}{\left(T_{i,j}^{n+1} - T_{i,j}^{n}\right)} & \left(T_{i,j}^{n+1} - T_{i,j}^{n}\right) \geq \varepsilon \\ c_{eff_{i,j}}\left(T_{i,j}^{n+1}\right) & \left(T_{i,j}^{n+1} - T_{i,j}^{n}\right) < \varepsilon \end{cases} \tag{76}$$

where $c_{eff_{i,j}}\left(T_{i,j}^{n+1}\right)$ means that specific heat depends on temperature.

After the correction is set we have to again recompute the temperature in future time, now with correct specific heat and we repeat the process to the end.

6.3 Numerical formulation of temperature recovery method

Last method studied in this thesis is the temperature recovery method. As mentioned in 4.3.3, it operates in two steps. To get to the first step, we have to prepare our temperature field of the first slice by using initial condition and we have to recompute our edge nodes using boundary condition. After we are done, we proceed to solve (46), which is discretized as follows:

$$\begin{aligned} \rho_{i,j} c_{i,j} \frac{T_{i,j}^{n+1} - T_{i,j}^{n}}{\Delta t} &= k_{i,j} \left(\frac{T_{i-1,j} - 2T_{i,j} + T_{i+1,j}}{(\Delta x)^2} + \frac{T_{i,j-1} - 2T_{i,j} + T_{i,j+1}}{(\Delta y)^2} \right) \\ T_{i,j}^{n+1} &= \frac{k_{i,j} \Delta t}{\rho_{i,j} c_{i,j}} \left(\frac{T_{i-1,j} - 2T_{i,j} + T_{i+1,j}}{(\Delta x)^2} + \frac{T_{i,j-1} - 2T_{i,j} + T_{i,j+1}}{(\Delta y)^2} \right) + T_{i,j}^{n} \end{aligned} \tag{77}$$

When the temperature $T_{i,j}^{n+1}$ gets to the mushy area, we need to correct it due to the latent heat generation. According to [17] there are five situations which can be encountered in numerical calculations and every one needs to be handled individually.

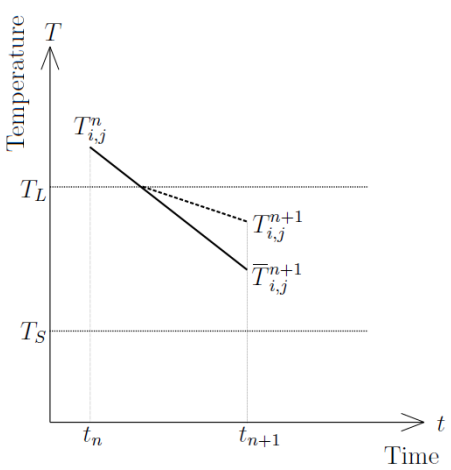

(a) Case 1

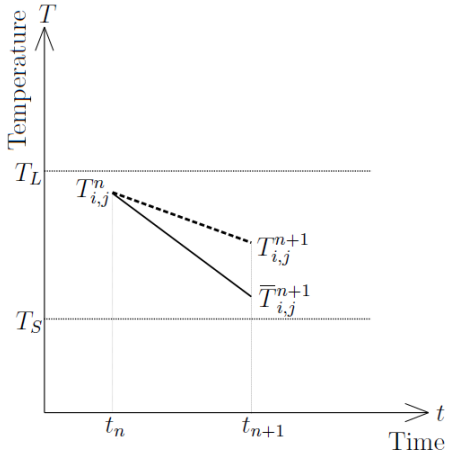

(b) Case 2

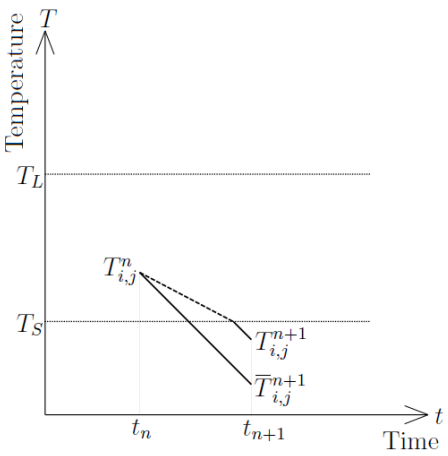

(a) Case 3

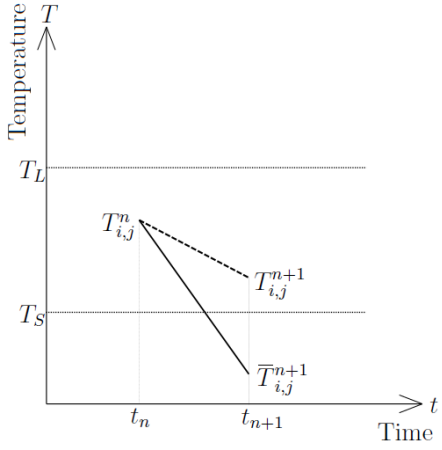

(b) Case 4

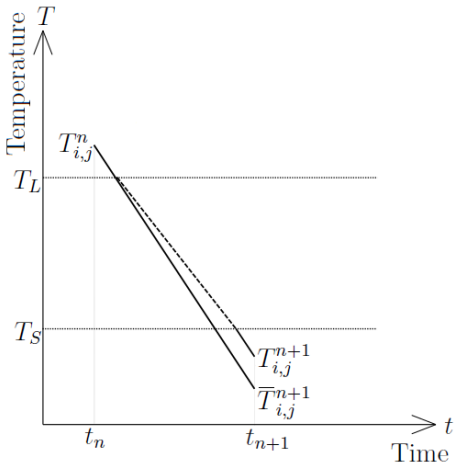

(c) Case 5

Figure 40: Five situations of temperature correction.

Corrections for the cases 1-5 as follows:

$$
\begin{aligned}
&\text{Case 1:} && T^{n+1}_{i,j} = \frac{c_{i,j}\overline{T}^{n+1}_{i,j} + \frac{L}{\Delta T}T_L}{c_{i,j} + \frac{L}{\Delta T}} \\
&\text{Case 2:} && T^{n+1}_{i,j} = \frac{c_{i,j}\overline{T}^{n+1}_{i,j} + \frac{L}{\Delta T}T^n_{i,j}}{c_{i,j} + \frac{L}{\Delta T}} \\
&\text{Case 3:} && T^{n+1}_{i,j} = \overline{T}^{n+1}_{i,j} + \frac{L\left(T^n_{i,j} - T_S\right)}{c_{i,j}\Delta T} \\
&\text{Case 4:} && T^{n+1}_{i,j} = \frac{c_{i,j}\overline{T}^{n+1}_{i,j} + \frac{L}{\Delta T}T^n_{i,j}}{c_{i,j} + \frac{L}{\Delta T}} \\
&\text{Case 5:} && T^{n+1}_{i,j} = \overline{T}^{n+1}_{i,j} + \frac{L}{c_{i,j}}
\end{aligned}
\tag{78}
$$

where $\overline{T}^{n+1}_{i,j}$ is the temperature in future time step $n+1$ computed without latent heat

addition; ΔT here means the difference between liquid (T_L) and solid (T_S) temperatures; $c_{i,j}$ depends on temperature $\overline{T}_{i,j}^{n+1}$, $c_{i,j} \equiv c_{i,j}\left(\overline{T}_{i,j}^{n+1}\right)$ and $T_{i,j}^{n+1}$ is our aimed future corrected temperature.

We can implement this method another way, when we have the enthalpy-temperature relation. By subtracting latent heat generated in structural and phase changes, we find a different enthalpy-temperature dependence. Then we will use both of them to compute and correct $T_{i,j}^{n+1}$.

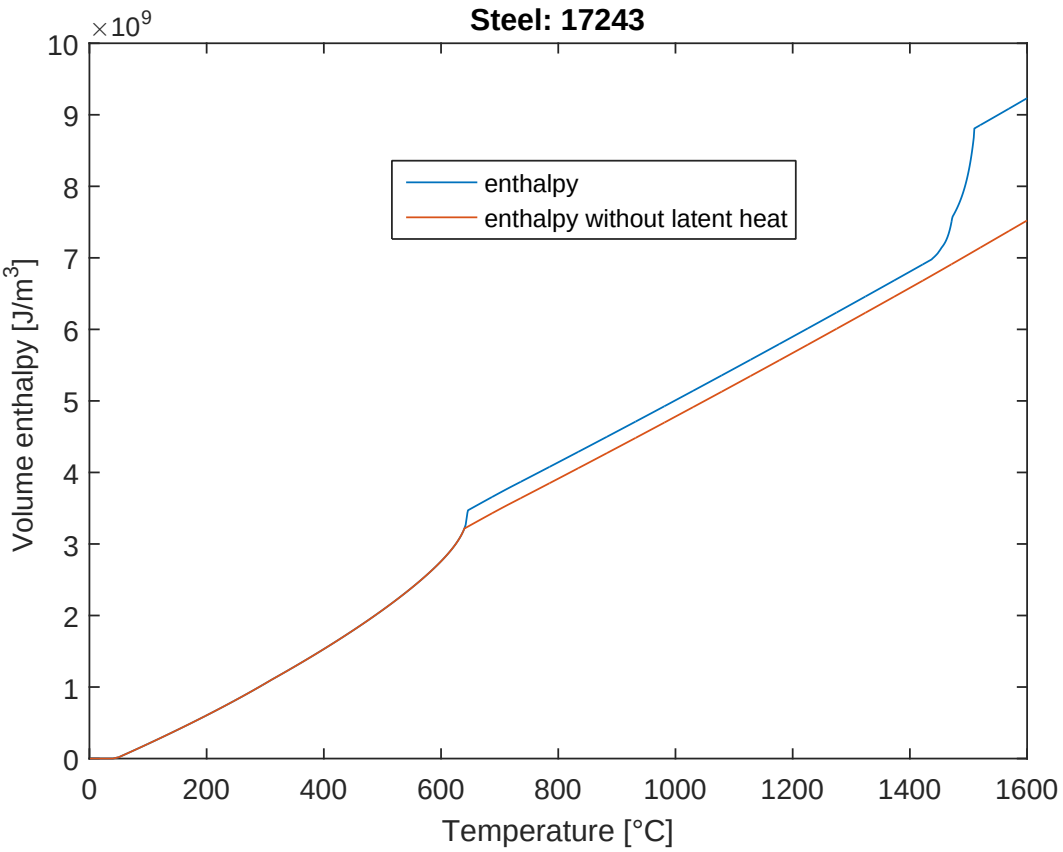

Figure 41: Known enthalpy-temperature relation with and without latent heat for steel 17243.

We compute $\overline{T}_{i,j}^{n+1}$ according to (77) and by utilizing the enthalpy-temperature relation depicted in figure 41 we obtain enthalpies $\overline{H}_{i,j}^{n+1}$, $\overline{H}_{i,j}^{n}$ and $H_{i,j}^{n}$ where $\overline{H}$ are enthalpies, where we don't consider latent heat generation. From those three, we can evaluate future time step enthalpy $H_{i,j}^{n+1}$ accordingly:

$$H_{i,j}^{n+1} = H_{i,j}^{n} - \left(\overline{H}_{i,j}^{n} - \overline{H}_{i,j}^{n+1}\right), \tag{79}$$

where from $H_{i,j}^{n+1}$ we obtain future time step $T_{i,j}^{n+1}$ using enthalpy-temperature relation and then we repeat the process for every time step till the end.

7 Results

Let us now introduce the results, concerning the numerical model of continuous casting of steel with slab design. Throughout this thesis, various methods of modeling latent heat have been presented. Therefore we will create a summarizing tables comparing these methods.

Dimensions of the slab slice were 1530x250 mm. Since the slab is axially symmetric, we modeled only the second half of it using adiabatic boundary condition on a symmetry axis. Model represents casting of the steel ČSN 17243 (AISI 303, DIN 1.4305). All thermal properties were either experimental from VÍTKOVICE STEEL, a.s. or computed by IDS program for steel compound identical to ČSN 17243. Model was computed for different mesh sizes (Table 1), with same casting speed $v = 0.8\text{m/min}$ using MATLAB environment.

Temperature field in representative points for various phase modeling methods with different grid size resulted in the following:

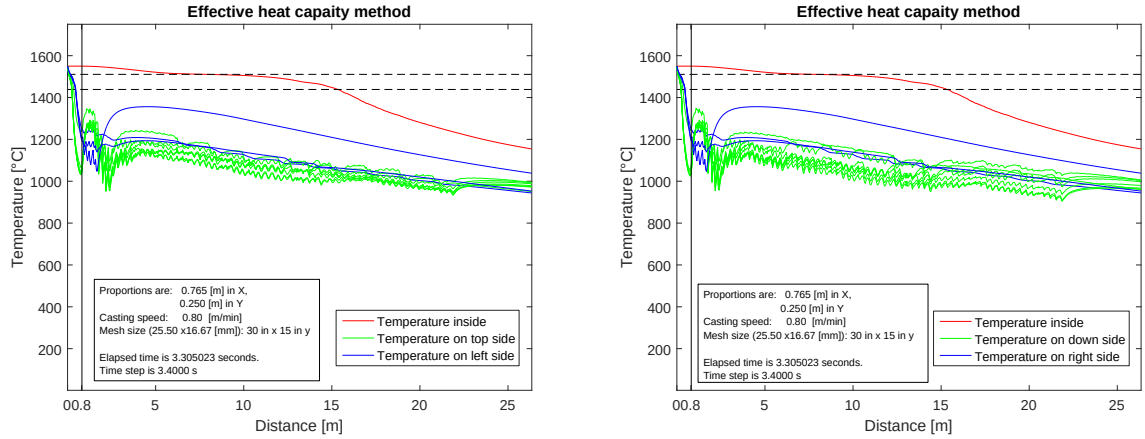

Figure 42: Effective heat capacity method on coarse mesh.

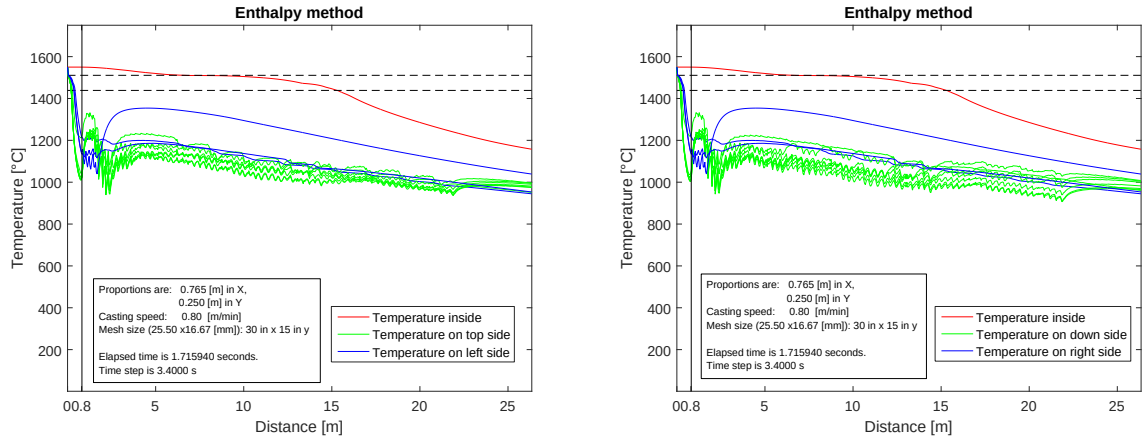

Figure 43: Enthalpy method on the coarse mesh.

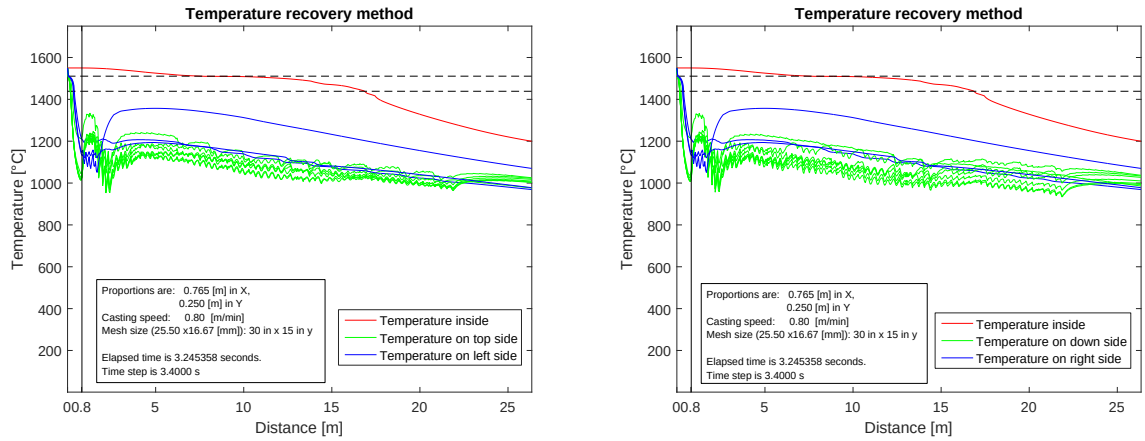

Figure 44: Temperature recovery method on coarse mesh.

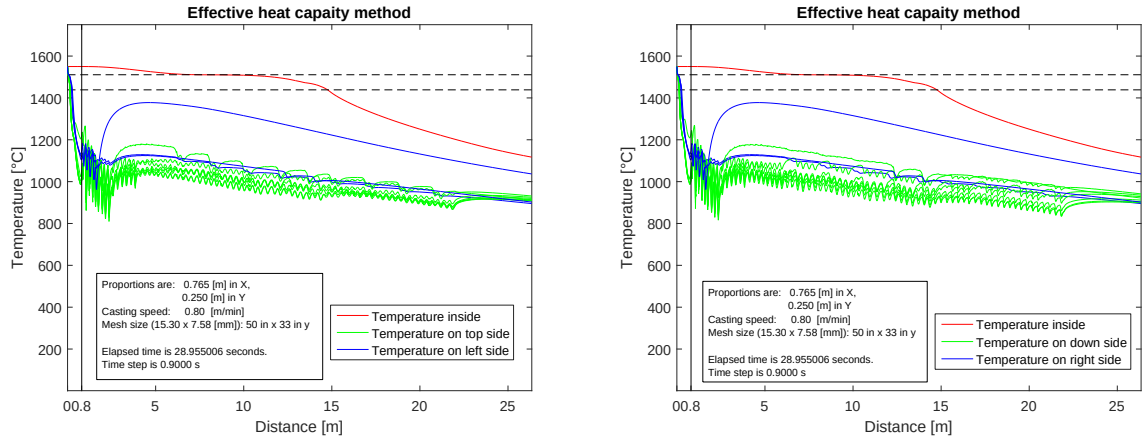

Figure 45: Effective heat capacity method on regular mesh.

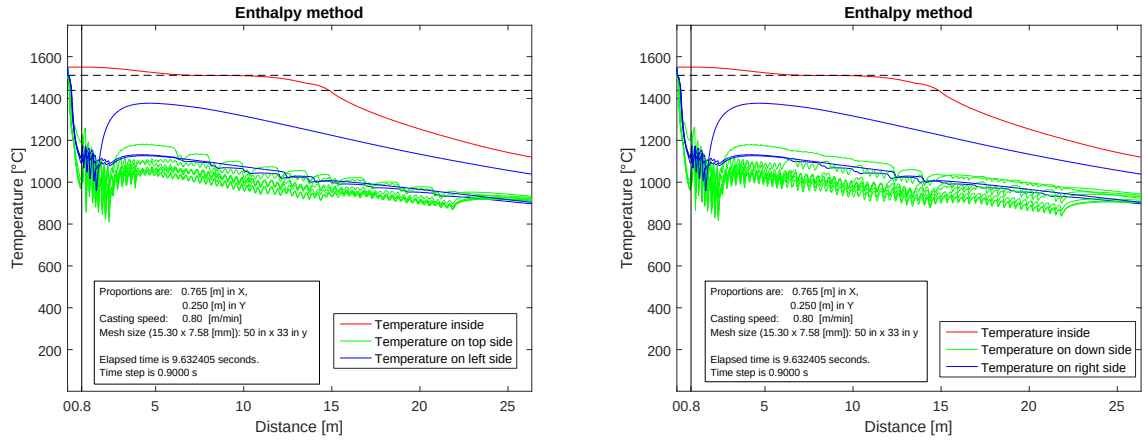

Figure 46: Enthalpy method on regular the mesh.

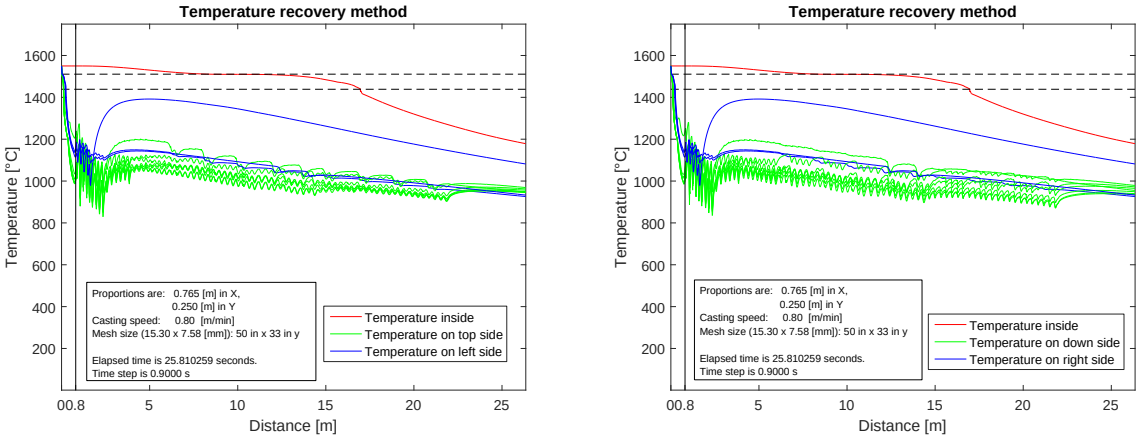

Figure 47: Temperature recovery method on regular mesh.

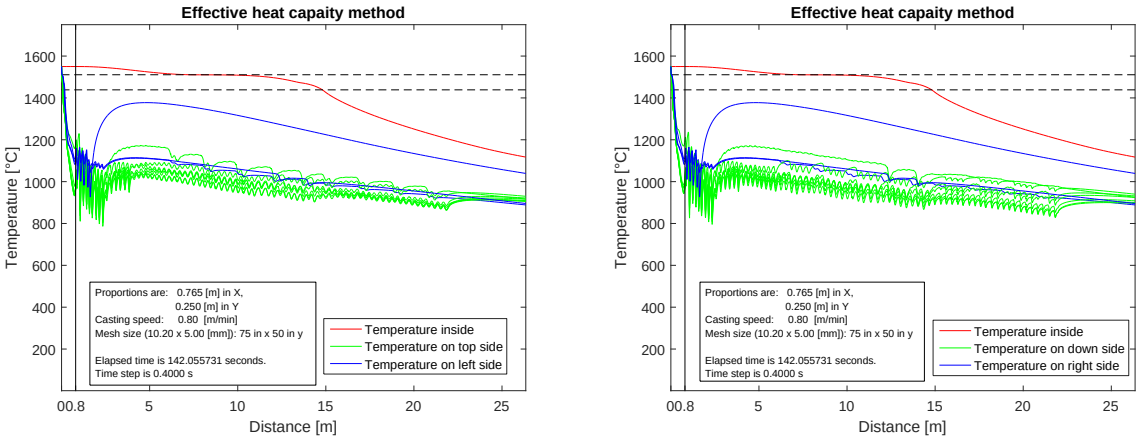

Figure 48: Effective heat capacity method on fine mesh.

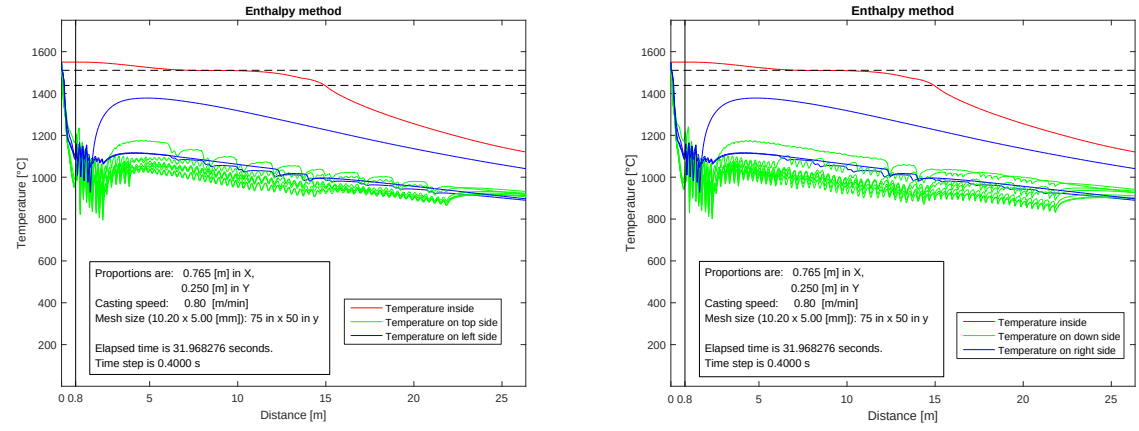

Figure 49: Enthalpy method on fine the mesh.

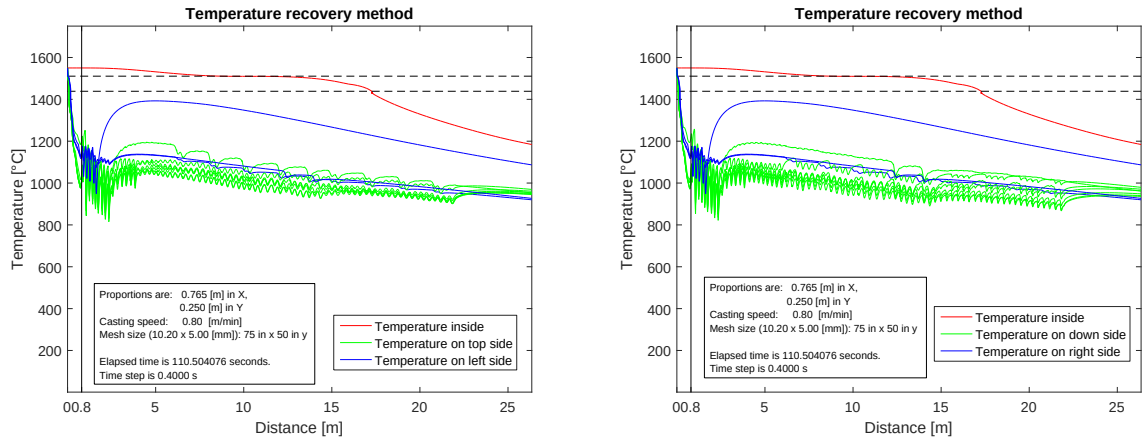

Figure 50: Temperature recovery method on fine mesh.

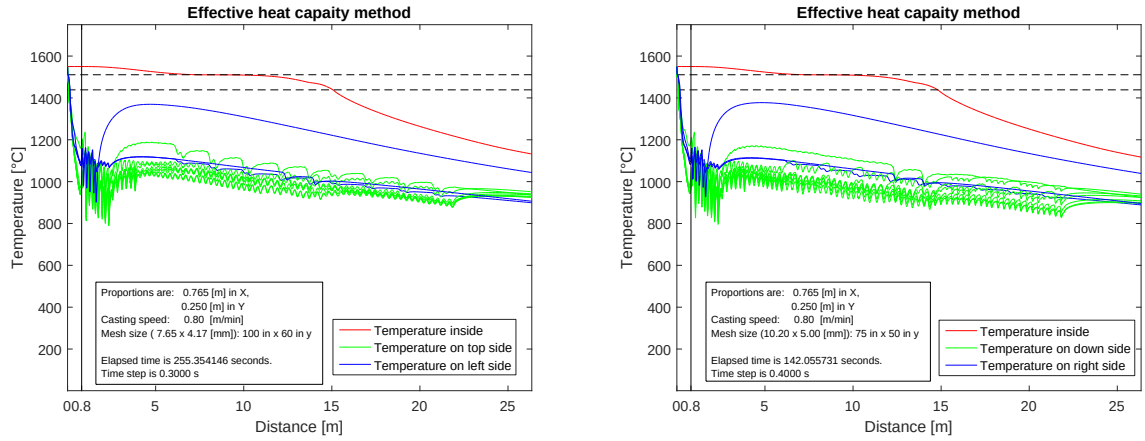

Figure 51: Effective heat capacity method on the finest mesh.

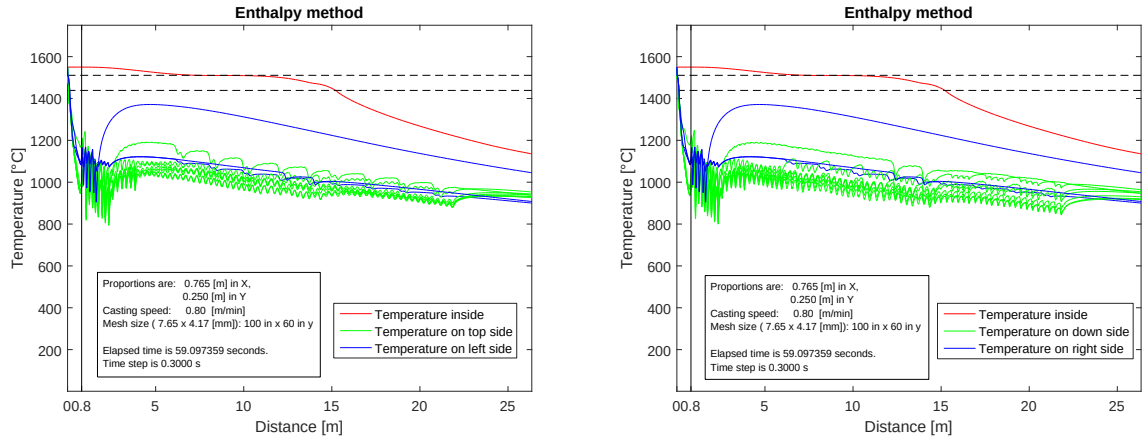

Figure 52: Enthalpy method on finest the mesh.

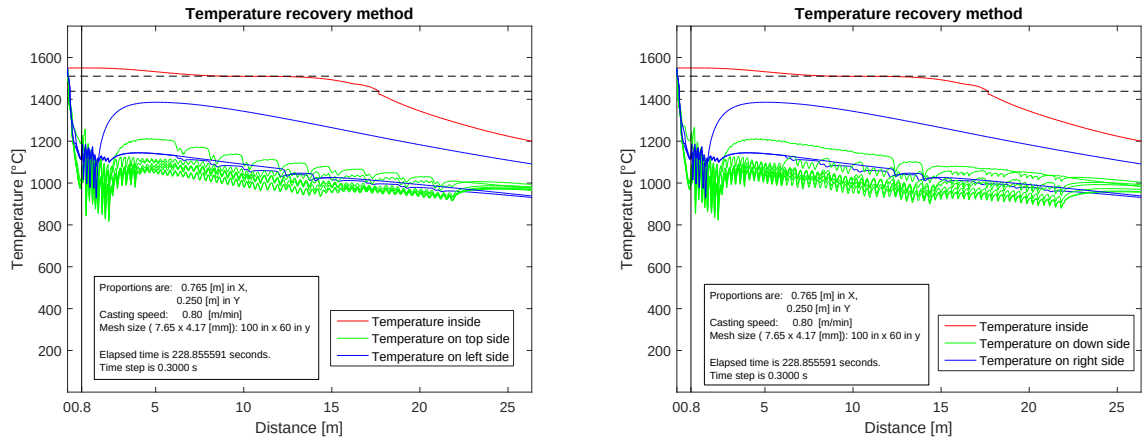

Figure 53: Temperature recovery method on the finest mesh.

Types of mesh:		
	Number of points for half slice (765x250):	Resulting dimensions (x,y):
Fine:	75x50	10.2x5 [mm]
Finest:	100x60	7.65x4.17 [mm]
Regular:	50x33	15.3x7.58 [mm]
Coarse:	30x15	25.5x16.67 [mm]

Table 1

Table of average computational time [s]			
Method:	Effective heat capacity	Enthalpy	Temperature recovery
Coarse mesh	3.8604	2.1283	3.3160
Regular mesh	29.6298	9.7002	28.8311
Fine mesh	129.2818	31.9168	106.8216
Finest mesh	255.1200	59.3835	208.1280

Table 2

Results presented in (Table 2) were obtained on Intel(R)Core(TM) i7-4702MQ CPU @2.20 GHz.

To present results connected to the error of metallurgical length of the strand applying various methods, we have to know the exact solution. Unfortunately, no such solution exists due to the complexity of the whole problem. However, we will assume the solution on the enthalpy method as the exact one, because the method was previously reported [6], [12] to be the most precise of all three. Authors applied various interface capturing as well as interface tracking phase change modeling methods on one and two phase Stefan's problems where the 1D solution is known. Utilizing their results and our assumption about the exact solution we get (Table 3):

	Error in metallurgical length of the strand [m]		
	Enthalpy method	Effective heat capacity	Temperature recovery
Coarse mesh:	2.3820	2.3830	2.350
Regular mesh:	1.5150	1.5230	1.3550
Fine mesh:	0	0.0270	0.3970
Finest mesh:	0.9570	0.9220	1.5190

Table 3

We also derived the evaluation of the temperature error when slice leaves the mold on y symmetry axis (Table 4).

	Average temperature error on symmetry axis y [°C]		
	Enthalpy method	Effective heat capacity	Temperature recovery
Coarse mesh:	16.5432	10.3397	14.3134
Regular mesh:	4.80407	1.7155	0.6417
Fine mesh:	0	2.3317	5.8963
Finest mesh:	1.0446	2.2085	7.2814

Table 4

Results for the continuous casting of steel ČSN 17243 show that the enthalpy and effective heat capacity method are comparable. Different results for temperature recovery method may be caused by its higher sensitivity to time step. Equations (58 - 61), are used for correct determination of time step size for linear problems. For the non-linear ones it is hard to find correct analytical constraint preserving the numerical stability. Despite of the fact, that linear stability conditions are not sufficient for non-linear problems shown by [8], they are still used, at least as an initial guess of the time step.

One possibility of avoiding this problem is to use a different discretization method, for example the implicit method or the Crank-Nicolson method, which were proven to maintain stability with arbitrary time step. Advantage of these methods is redeemed in increasing number of total iterations necessary to preserve the stability. Short overview is in the table (Table 5), where more information can be found in [16].

	Discretization methods		
	Explicit method	Implicit method	Crank-Nicolson method
Stability	not always	allways	allways
Truncation error	$O(\Delta t)$	$O(\Delta t)$	$O((\Delta t)^2)$
Pros	Straightforward implementation, less CPU cost	Unconditional stability	Smaller Truncation error, unconditional stability
Cons	Conditional stability	Time consuming	Equations needs to be solved simultaneously which is time consuming

Table 5

Another possible reason of bigger error appearance is the fact, that we did not have

exact temperatures for the beginning and end of the structural changes. Therefore the recalculation of properties during structural changes was not correct.

For further application of the slice model for continuous casting, implicit or semi-implicit discretization would be more suitable, if we wanted to be sure about stability. In this case stability would be preserved and the potentially higher number of steps needed for the convergence of the calculation would not affect the overall computation time as much as in the case of a 3D model. Furthermore, additional reduction of computational time may be achieved by utilizing parallel computation.

Requirements nowadays usually demand the shortest possible computation times and the finest possible grid resolutions. These two parameters are the two key driving factors in the contemporary online optimization of the continuous casting of steel and the regulation of this process. Hence the prediction of temperature field by numerical models is necessary for the control of casting parameters. Following are a few possible ways of parallelization:

- Enthalpy method:
  1. Computing thermophysical parameters for specific temperatures.
  2. Computing new enthalpies in time $t_i + \Delta t$ from the enthalpies in time t_i.
  3. Converting enthalpy in $t_i + \Delta t$ to temperature in $t_i + \Delta t$.
- Effective heat capacity method:
  1. Preparing thermophysical properties in corresponding temperatures.
  2. Computing the temperature in imaginary nodes $i = 0$ and $i = n + 1$ via boundary conditions.
  3. Evaluating the temperatures in new time step $t_i + \Delta t$.
- Temperature recovery method:
  1. Computing thermophysical properties in corresponding time.
  2. Determine the temperature of imaginary nodes $i = 0$ and $i = n + 1$ using boundary conditions.
  3. Transforming temperatures to enthalpies without latent heat using temperature-enthalpy relation.
  4. Computing temperature $\overline{T}$ in $t_i + \Delta t$.
  5. Evaluate corresponding enthalpy with latent heat in $\overline{T}$.
  6. Obtain temperatures in next time step $T_i + \Delta t$.

When we want to compute the process in parallel, it is usually better to work with simple explicit method, because the scheme is parallel in nature. Meaning that the temperature field is calculated only from previous results, hence space dimensions can be distributed over an arbitrary number of processors. More about parallelization can be found in [12], [6], [18].

Note that significant portion of time during parallel execution is consumed by data transfer between CPU workers. For small problems, this time may be even bigger than the time of a corresponding to sequential solution, making parallelization inadequate.

8 Conclusion

The goal of the thesis was to develop a 2D nonlinear phase change heat transfer model with moving boundary conditions, using several different approaches for modeling of the phase change and compare the results.

These goals were accomplished in the implementation of enthalpy method, effective heat capacity method and temperature recovery method. Subsequent evaluation of these methods concluded that enthalpy and effective heat capacity methods provide comparable results, while slightly different results for temperature recovery method were attributed to its higher sensitivity to a size of a time step around mushy area.

Also the 2D slice model with moving boundary conditions studied in this thesis reflect a real geometry of caster used by VÍTKOVICE STEEL, a.s. This model set a foundations for more robust future slice models for VÍTKOVICE STEEL, a.s. For example for models concerning also tightness in steel.

This work was able to present a practical working solution to the problem of continuous casting of steel ČSN 17243. However, only by changing of entry data we can obtain results for different steel.

The thesis led to an deeper understanding of problems connected with phase change, numerical implementation of the mathematical models, working with real world data and overall better understanding of continuous casting process.

One of the possible future extensions of this work may be implementation of implicit or semi-implicit discretization methods, or comparison od 2D slice model to the fully 3D model.

References

[1] BERTOLA, V. An Experimental Study Of Bouncing Leidenfrost Drops: Comparison Between Newtonian And Viscoelastic Liquids. *International Journal of Heat and Mass Transfer.* 2009;52:1786-1793. ISSN 0017-9310.

[2] BIRAT JP, et al. *The Making, Shaping and Treating of Steel: Casting Volume.* 11th ed. ALAN W. CRAMB. Pittsburgh, PA, USA: The AISE Steel Foundation, 2003. ISBN 0-930767-04-7.

[3] ÇENGEL, YA. *Heat Transfer: A Practical Approach.* New York, USA: McGraw-Hill Companies, 2002. ISBN 978-0-0724-5893-0.

[4] HA JS, et al. Numerical Analysis on Secondary Cooling and Builging in the Continuous Casting of Slabs. *Jurnal of Materials Processing Technology.* 2001;113:257-261. ISSN 0924-0136.

[5] IRVING, WR. *Continous casting of steel.* Leeds, United Kingdom: The Institute of Materials, 1993. ISBN 978-0-9017-1653-8.

[6] KLIMEŠ L, MAUDER T, CHARVÁT P, ŠTĚTINA J. Front tracking in modelling of latent heat thermal energy storage: Assessment of accuracy and efficiency, benchmarking and GPU-based acceleration. *ENERGY.* 2018;155:297-311. ISSN 0360-5442.

[7] KLIMEŠ L, MAUDER T, ŠTĚTINA J, CHARVÁT P. A 3D Front Tracking Slice Model for Continuous Casting of Aluminium. *Metal.* 2017;1813-1819 ISBN 978-8-0872-9473-4.

[8] KUZNIK F, VIRGONE J, ROUX JJ. Energetic efficiency of room wall containing PCM wallboard: A full-scale experimental investigation. *Energy and Buildings.* 2008;40:148–156.

[9] LALLY B, BIEGLER L, HENEIN H. Finite Difference Heat-Transfer Modeling for Continuous Casting. *Metallurgical Transactions.* 1990;21B:761–770. ISSN 1543-1916.

[10] LIU YC, CHAO LS. Modified effective Specific Heat Method of Solidification Problems. *Materials Transaction Journal.* 2006;47:2737–2744.

[11] MAUDER, T. *Optimalizace bramového plynulého odlévání oceli za pomoci numerického modelu teplotního pole:* Dizertační práce. Brno: Vysoké učení technické v Brně, Fakulta strojního inženýrství, 2012. Vedoucí práce prof. Ing. František Kavička, CSc.

[12] MAUDER T, CHARVÁT P, ŠTĚTINA J, KLIMEŠ L. Assessment of basic approaches to numerical modeling of phase change problems – accuracy, efficiency and parallel decomposition. *Journal of Heat Transfer.* 2017;139(8):1-5. ISSN 0022-1481.

[13] MIETTINEN J. *IDS Solidification Analysis Package for Steels: User manual of DOS version 2.0.0.* Helsinki, Finland: Helsinki University of Technology, 1999.

[14] PASCON F, CESCOTTO S, HABRAKEN AM. A 2.5D Finite Element Model for Bending and Straightening in Continuous Casting of Steel Slabs. *International journal for numerical methods in engineering.* 2006;68:125-149. ISSN 1097-0207.

[15] ŠARLER B, VERTNIK R, LORBIECKA AZ, VUŠANOVIĆ I, SENČIČ B. A multiscale slice model for continuous casting of steel. *IOP Conference Series: Materials Science and Engineering*. 2012;33:1-8.

[16] THOMAS, JW. *Numerical Partial Differential Equations: Finite Difference Methods. Texts in Applied Mathematics*. 22nd ed. Berlin, New York: Springer-Verlag, 1995. ISBN 978-0-387-97999-1.

[17] TSZENG TC, IM YT, KOBAYASHI S. Thermal analysis of solidification by the temperature recovery method. *International Journal of Machine Tools and Manufacture*. 1989;29(1):107-120.

[18] WALLNER, M. *Algebraic multigrid methods for higher-order finite element discretization with parallelization dissertation.* Master's thesis. London: Brunel University London, School of Information Systems, Computation and Mathematics, 2012. Supervised by Dr. Matthias Maischak.

[19] ZHANG Q, YANG L, WEN H. A mathematical modelling of heat transfer in continuous casting slab. *Applied Mechanics and Materials*. 2010;44-47:33-37.

List of Symbols

c_{eff}	[J/m^3]	Effective heat capacity
c_w	[J/kgK]	Specific heat capacity of water
f_s		Ratio between liquid and solid phase
htc_w	[W/m^{2}K]	Heat transfer coefficient for cooling water
k	[W/mK]	Thermal conductivity
L	[J/kg]	Latent heat
L	[m]	Thickness of mold areas
M_i	[kg/mol]	Molar mass
$\dot{q}$	[W/m^2]	Density of heat flow
$\dot{Q}$	[W/m^3]	Heat flux
Q^*	[W/m^3]	Rate at which energy is generated per unit volume of the medium
R	[m^{2}K/W]	Total heat resistance
S	[m^2]	Area of strand/roll contact
T	[K]	Temperature
V_m	[m^3/mol]	Molar volume
W	[l/m^{2}s]	Density of water flow
x_i		Volume fraction of the i-th component
ε		Emissivity
η		Viscosity
ρ_w	[kg/m^3]	Density of water
σ	[W/m^{2}K^4]	Stefan–Boltzmann constant
Gr		Grashof number
Nu		Nusselt number
Pr		Prandtl number
Re		Reynolds number

Abbreviation

CCM	Continuous casting machine

Attachment

Code.rar contains:

1. Diplomka-run.m
2. Enthalpy-run.m
3. Temperature-recovery-run.m
4. Effective-heat-capacity-run.m
5. Diplomka-run.m
6. temperatures.m
7. progressbar.m
8. entry data